Molecular and Cellular Mechanisms underlying Cardiac Autonomic Dysfunction in Rats with Traumatic Brain Injury

Jiwoong Oh

The Graduate School
Yonsei University
Department of Medicine

Molecular and Cellular Mechanisms underlying Cardiac Autonomic Dysfunction in Rats with Traumatic Brain Injury

Directed by Professor Kum Whang

A Dissertation
Submitted to the Department of Medicine,
and the Graduate School of Yonsei University
In partial fulfillment of the
requirements for the degree of
Doctor of Philosophy

Jiwoong Oh

February 2021

This certifies that the Doctoral Dissertation of

Jiwoong Oh is approved.

Thesis Supervisor: Kum Whang, M.D, Ph.D.

Seong-Woo Jeong, Ph.D.: Thesis Committee Member

Kwang Hwa Park, M.D., Ph.D.: Thesis Committee Member

Byung Ho Cha, M.D., Ph.D.: Thesis Committee Member

Ji-Yong Lee, M.D., Ph.D.: Thesis Committee Member

The Graduate School

Yonsei University

February 2021

ACKNOWLEDGEMENTS

This dissertation has been contributed by multiple efforts from many people around me. Firstly, I would like to show my deep gratitude to Professor Kum Whang and Professor Seong-Woo Jeong. You both are admirable researchers as teachers. My graduate school training was hard but also very enjoyable with tremendous amount of scientific and clinical learning from you all. Thank you whole-heartedly for your patience, guidance, and encouragement throughout my PhD course.

My sincere thanks also go to my committee members - Professor Ji-Yong Lee, Professor Kwang Hwa Park, and Professor Byung Ho Cha - for their constant guidance, critique, and moral input so that I do not give up my PhD degree.

I am indebted to my good friend, Chung-Ku Lee, for walking with me throughout my scientific career at the Department of Physiology. For numerous days and nights, we did not sleep to solve many difficult problems during designing and carrying out the experiments in our PhD degree together. These experiments were something we have never done before so we struggled painfully but the outcome was rewarding. We studied and endured hard time together to troubleshoot and to move forward with scientific solution. As a person who had no idea what basic research was, I started everything from the scratch and from the bottom as an apprentice. I learned how to pipette, to read basic science papers with puzzles of

molecular biochemistry, to grow cultures of primary neurons, to patch-clamp cells, to extract RNA to make cDNA for PCR, to stain brain tissues with immunohistochemical tools, and to make TBI animal models related to my special field - trauma neurosurgery. All of this has been a delightfully valuable time which I will remember and treasure for the rest of my life.

I am obliged to give huge thanks to my parents. My mother and father supported me and encouraged me to pursue my dreams as clinical researcher with scientific skills and minds. My present state is impossible if there were no countless sacrifices from my parents. I hope I have made you proud as your son. I also give an equivalently large thanks to my big brother, Jiyoung, and little sister, Jihyun, for your endless support and mentoring from the beginning of this journey.

I am truly fortunate to get married during my PhD degree and I should never forget to thank my wife, Sohyun, my daughter, Saedahm, and my son, Saehahm. They understood me well with patience without any grudge or criticism against me (I hope, and I believe). My thirties were spent most of time in the hospital with neurosurgical patients and in the lab with my PhD degree. I spent less time with my beloved family members – this is the hurting fact of my current situation. Nevertheless, my family has loved me and is still loving me for what I am. The pressures I went through was overcome nicely and smoothly because of my family's tremendous love, understanding, laughter, and unconditional support. I thank you all and I love you all.

Finally, but not the least, I would like to faithfully thank the lab mates from the Department of Physiology and the colleagues from the Department of

Neurosurgery in Wonju College of Medicine, Yonsei University, for their help, care, and support so that I did not feel lonely in this journey of PhD. As a neurosurgeon, doing a basic research for a PhD degree was not easy at all. I was not good enough most of time, but I tried my utmost best to finish what I started. I have many good memories to remember and valuable experiences against the challenges during my PhD and I have no regrets.

February 2021

Jiwoong Oh

CONTENTS

LIST OF FIGURES

LIST OF TABLES

ABBREVIATIONS

AB	Arterial baroreceptor
ACh	Acetylcholine
AD	Autonomic dysfunction
ADN	Aortic depressor nerve
AHP	Afterhyperpolarization
AMPA	α-amino-3-hydroxy-5-methyl-4-isoxazolepropionic acid
ANG II	Angiotensin II
AT1R	Angiotensin type 1 receptor
AP	Action potential
ASICs	Acid-sensing ion channels
AV	Atrioventricular
BRS	Baroreflex sensitivity
CaV	Voltage-gated calcium channels
cAMP	Cyclic adenosine monophosphate
CCl4	Carbon tetrachloride
CNS	Central nervous system
CO	Cardiac output
COX	Cycloxygenase
CVLM	Caudal ventrolateral medulla
Di-I	1,1'-Didodecyl-3,3,3',3'-tetramethylindocarbocyanine perchlorate
DRG	Dorsal root ganglion
DMSO	Dimethyl sulfoxide
EBSS	Earle's balanced salt solution
ECG	Electrocardiography
ENaC	Epithelial Na^+ channels
FBS	Fetal bovine serum

HBSS	Hanks' Balanced Salt Solution
HCN	Hyperpolarization-activated cyclic nucleotide channels
HF	High frequency
HR	Heart rate
HRV	Heart rate variability
I.P.	Intraperitoneal injection
ICG	Intracardiac ganglion
IgG	Immunoglobulin G
IML	Intermediolateral cell column
K_A	Transient (A-type) potassium
K_{ca}	Calcium-dependent potassium
KCNQ	Voltage-gated potassium channel subfamily Q member
K_{DR}	Delayed rectifier potassium
K_M	Muscarinic (M-type) potassium
KTDBS	Korean Trauma Data Bank System
K_V	Voltage-dependent potassium
LF	Low frequency
mAHP	Medium afterhyperpolarization
MAP	Mean arterial pressure
MMPs	Matrix metalloproteinases
NA	Nucleus ambiguus
Na_V	Voltage-gated sodium
NE	Norepinephrine
NF-κB	Nuclear factor kappa-light-chain-enhancer of activated B cells
NG	Nodose ganglion
NMDA	N-Methyl-D-aspartic acid
NMDG	N-methyl-D-glucamine
NO	Nitric oxide
NTS	Nucleus tractus solitarius
PCR	Polymerase chain reaction
PE	Phenylephrine

PG	Petrosal ganglia
PI	Pulse interval
Ri	Input impedance
RMP	Resting membrane potential
RVLM	Rostral ventrolateral medulla
RT-PCR	Reverse transcription polymerase chain reaction
SA	Sinoatrial
sAHP	Slow afterhyperpolarization
SCG	Superior cervical ganglion
SDNN	Standard deviation of normal to normal interval
SNP	Sodium nitroprusside
SG	Stellate ganglion
SNS	Sympathetic nervous system
SPNs	Sympathetic premotor neurons
TAA	Thioacetamide
TEA	Tetraethylammonium
TPR	Total peripheral resistance
TRP	Transient receptor potential
TRPV	Transient receptor potential vanilloid
VGCC	Voltage-gated calcium channels

ABSTRACT

Molecular and Cellular Mechanisms underlying Cardiac Autonomic Dysfunction in Rats with Traumatic Brain Injury

Jiwoong Oh

Department of Medicine

The Graduate School

Yonsei University

Traumatic brain injury (TBI) frequently causes cardiac autonomic dysfunction (CAD), irrespective of its severity, which is associated with an increased mortality in patients. Despite the effort to study the cellular mechanism underlying TBI-induced CAD, animal models on this mechanism are lacking. In the current study, I examined whether CAD is developed during the post-insult sub-acute period in a controlled cortical impact rat model of TBI. The severity of TBI was evaluated via quantification of the cortical lesion volume. Power spectral analysis in the frequency domain of heart rate variability (HRV) showed that the low frequency (LF) / high frequency (HF) ratio was increased in moderate and severe TBI rats. On the other hand, the measurement of the reflexive bradycardia during vasoconstrictor induction that the baroreflex sensitivity (BRS) was reduced

in moderate and severe TBI rats. Overall, the higher LF/HF ratio and lower BRS observed in the TBI rats suggest an autonomic imbalance with sympathetic hyperactivity and parasympathetic hypoactivity. Then, cell excitability was recorded in the sympathetic stellate ganglion (SG) neurons and parasympathetic intracardiac ganglion (ICG) neurons using the gramicidin-perforated patch-clamp technique. The number of action potential (AP) discharges was significantly increased in the SG neurons and decreased in the ICG neurons in TBI rats, compared to the sham rats. The hyperexcitability of the SG neurons and the hypoexcitability of the ICG neurons in TBI rats are associated with the decreases and increases in the AP threshold and duration, respectively. The transient A-type K^+ (KA) currents, but not the delayed rectifying K^+ currents were significantly decreased in SG neurons in TBI rats, compared with sham animals. Consistent with these electrophysiological data, the transcripts encoding the Kv4 α subunits (Kv4.1, Kv4.2, and Kv4.3) were significantly downregulated in SG neurons in TBI rats, compared with sham rats. The application of XE-991, a selective M-type K^+ (KM) channel blocker, increases the number of AP discharges in SG and ICG neurons. TBI causes the downregulation and upregulation of functional KM currents and the KCNQ2 mRNA transcripts, which may contribute to the hyperexcitability of the SG neurons and the hypoexcitability of the ICG neurons, respectively. In addition, TBI was found to affect the afferent limb of the baroreflex arc by dramatically decreasing the excitability of both A- and C-type baroreceptor neurons. In conclusion, the CAD was developed during post-insult sub-acute period in a rat model of TBI.

The key cellular mechanism underlying the TBI-induced CAD may be the functional plasticity of the peripheral cardiac efferent neurons, which is caused by the regulation of the K_A and/or K_M currents, and cardiac afferent neurons.

Keyword: autonomic dysfunction, baroreflex sensitivity, cardiac autonomic dysfunction, heart rate variability, intracardiac ganglion, parasympathetic, potassium channel, stellate ganglion, sympathetic, traumatic brain injury

I. INTRODUCTON

1.1 Traumatic brain injury (TBI)

1.1.1 Classification of TBI

Traumatic brain injury (TBI), which is defined as an acquired brain injury by the application of sudden mechanical forces, is the leading cause of mortality in human race (Coronado et al., 2011). TBI can be classified based on severity (ranging from mild to severe TBI), mechanisms (closed or penetrating head injury), or other features (e.g., focal or global) (Kobayashi, 1982; Lai et al., 2020). To be more specific, the types, injury duration, degree of brain injury attribute to the severity of TBI. Types of the brain damages are as follows: angular, shear, translational, and rotational injuries (Punchak et al., 2018). A standard classification of the severity of injury in TBI is initially evaluated by Glasgow Coma Scale (GCS). GCS scores are world-widely accepted scoring system and are defined as follows: severe TBI (3-8); moderate TBI (9-12); and mild TBI (13-15). TBI-related animal models for research have also applied and modified such system to classify the severity of injury (Ma et al., 2019).

1.1.2. Epidemiology of TBI

TBI is a non-neurodegenerative neurosurgical disease. TBI is one of the leading causes of deaths accounting for almost 30-40% of all mortalities from acute injuries. World widely, more than 60 million incidences of TBI occur

each year (Maas et al., 2017). TBI survivors experience many clinical complications ranging from neurological, psychosocial problems to long-term disability (Bazarian et al., 2009). The financial costs of TBI are estimated to be over $70 billion per year internationally. This ultimately affected the economic states of the patients and family caregivers due to the inclusion of medical and rehabilitation care and continuous costs related to this care. The rate of mortality is evidently extremely high as 17 per 100,000 people are reported to be the current statistics. This is almost 7-8 per 100,000 people for patients in the hospitals (Faul et al. 2015). After all, this results in many socio-economic burdens due to an immense medical expense. To set up a systematic protocol in managing TBI, for instance, South Korea, has recently set up Korean Trauma Data Bank System (KTDBS) so that the clinicians can find the correlation between the critical parameters and functional prognosis after TBI (Jeong et al., 2016). Yet, more data must be collected to prevent TBI as well as to treat the patients with minimal secondary injury with neurologic deficits.

1.1.3. Pathophysiology of TBI

1.1.3.1. General view

Understanding the underlying pathophysiological mechanisms of TBI has an important implication of developing therapeutic plans for preclinical and clinical studies.

TBI is categorized largely into two sub-classifications: (i) primary injury,

which is directly caused by mechanical forces during the initial insult; and (ii) secondary injury, which refers to further tissue and cellular damages following primary insult.

Mechanical input at the time of brain damage causes an initial primary brain injury which activates a secondary brain injury. This subsequently results in an increase in the intracranial pressure and a decrease in the cerebral perfusion. Primary injury is a critical factor for final prognosis of the patients with TBI. (Perez-Alfayate et al., 2019; Tapper et al., 2017) Thus, the goal of treating TBI is the prevention of either primary injury (i.e., preventing the traumatic events to happen in the first place) or the progression of secondary injury. An initial primary brain injury rapidly activates devastating secondary brain injuries including cerebral ischemia, increased intracranial pressure (ICP), and reduced cerebral blood flow (CBF) (Fig. 1). After primary injury, the cerebrovascular flow retention occurs due to intracranial hypertension, and this ultimately causes the global or local cerebral ischemia in the brain. Subsequently, the secondary ischemic insults will follow the primary injury. Although inflammation at the injury sites increases the oxygen consumption, the reduced CBF decreases the brain oxygen delivery, which determines the degree of secondary ischemic insults and the outcome of the TBI patient. The secondary injuries are often reversible and modifiable with immediate treatment in a timely manner (Baguley et al. 2008). The more details of the mechanisms of secondary injuries including many inflammatory changes induced by the trauma are described in the following section. After all, there is a whole spectral range of damage in TBI and the process in

between the start and the end stage of the disease determine the prognostic aspect of the patients.

1.1.3.2. Biochemical and cellular mechanisms of the secondary brain injuries

Secondary changes of the normal brain tissue may develop in tissues with direct impact or in the opposite to the contusion due to the striking, shearing, and stretching by brain rebounds, hence disruption of gap junctions in the brain structure (Schmidt et al., 2004, Pearn et al., 2017). The extent of neurologic deficits such as cognitive impairments and motor hemiparesis is normally determined by this impact. Consequently, abnormal mechanistical forces damage neuronal axon circuits, blood vessels, leading to brain edema and ischemic brain damage (Smith et al., 2003). Subcellular events occur where the neuronal damages are followed by the uncontrolled influx of ions such as sodium and calcium due to the breakage of plasma membrane of neurons and other structural cells (Pearn et al., 2017). Dysregulated influx of calcium into the injured cells initiates a vicious cycle of cellular toxicity with over release of glutamate which causes further cytoplasmic calcium increase. This eventually leads to mitochondrial dysfunction at the cellular level with the production of reactive oxygen species (ROS) and cell death (Pearn et al., 2017; McDonald et a., 2020). Notably, the axonal damages can persist up to months following TBI, suggesting an association with delayed secondary pathology of hemorrhages and brain edema (Saatman et al.,

2008). Secondary brain injuries initiate as soon as primary injury is progressed, so the overall impact is not sequential, but rather a continuum of different mechanisms of injuries. There are several types of secondary injuries and some are mentioned as follows: (1) brain blood barrier destruction leading to the release of excitatory amino acids and causing excitotoxicity (Chamoun et al., 2010); (2) mitochondrial dysfunction and metabolic derangements in dying neurons with the production of reactive oxygen species, and subsequent cell death such as apoptosis (Grady et al., 2003, Xiong et al., 1997, Singh et al., 2006); (3) neuroinflammation with overflooding of circulating cytokines such as IL-1β, IL-6 and TNF-α through the damaged blood brain barrier, into the damaged brain tissue (Lotocki et al., 2009); (4) global disorganization of axonal cytoskeletal network due to direct injury causing failures in the normal neural transmission (Povlishock, 2006); and (5) reactive gliosis mediated by astrocytes and microglia which make glial scars to inhibit the recovery of axonal injury (Fawcett et al. 1999) (Fig. 2). Detailed activated mechanisms of microglia and gliosis are not much studied in TBI. However, the activation of M1 and M2 phenotypes of microglia are suggested to be critical for the permanently changed environment of the injured brain (Pearn et al, 2019).

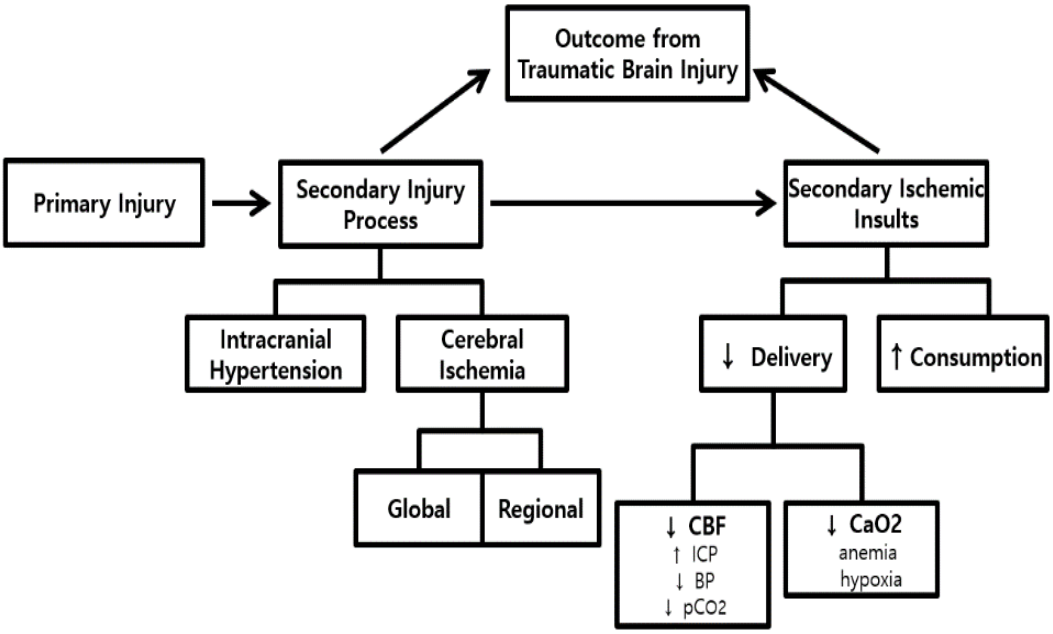

Figure 1. The secondary processes of TBI.

(BP: blood pressure; CBF: cerebral blood flow; ICP: intracranial pressure; TBI: traumatic brain injury)

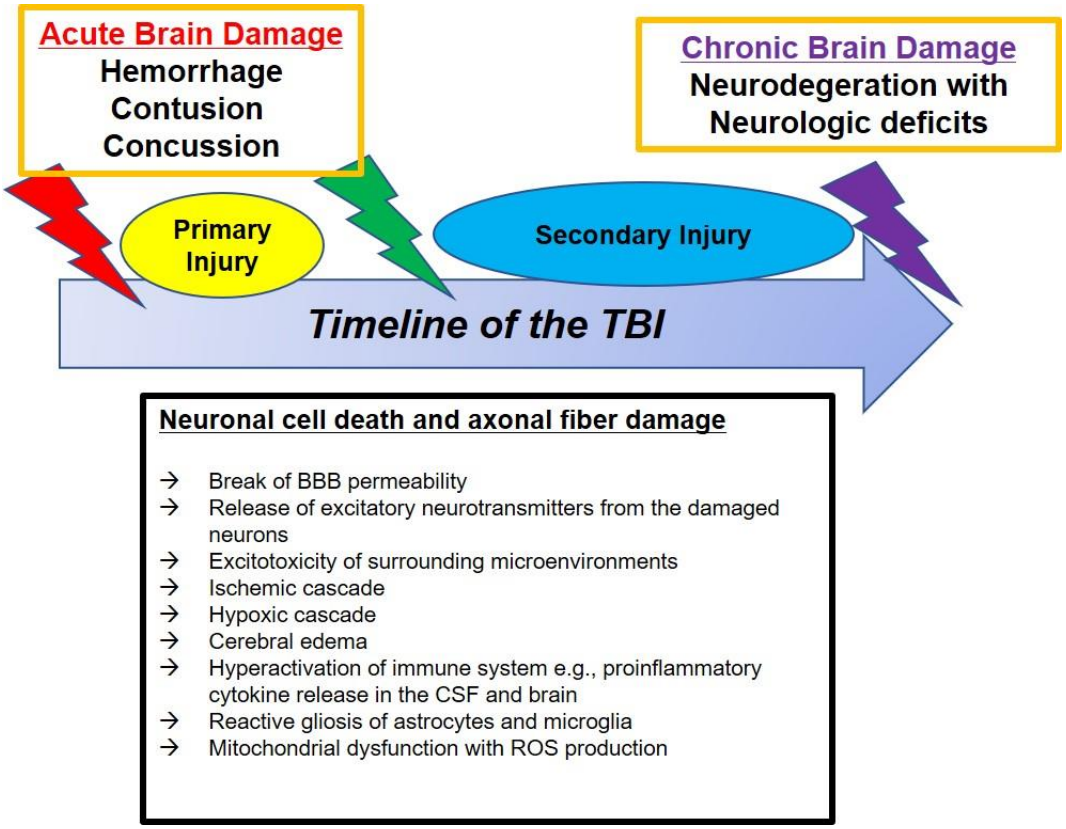

Figure 2. The potential biochemical and cellular mechanisms of the secondary brain injuries.

1.2. Cardiac autonomic nervous system (ANS)

The autonomic nervous system (ANS) is a part of peripheral nervous system where it controls smooth muscle contraction of heart, respiration, digestion, secretion of glands, renal functions (e.g., urination) and modulates the functions of internal organs (Wehrwein et al., 2016). The ANS is linked from the brainstem to the spinal cord and the related organs. The autonomic nervous system has three branches: the sympathetic nervous system, the parasympathetic nervous system and the enteric nervous system. The cardiac autonomic nervous system (cardiac ANS) is defined to contain sympathetic and parasympathetic nervous system of heart and it covers many physiological functions. It regulates heart rate, blood flow, and blood pressure. Major parts of my research focus on finding out how distinct neurons in peripheral autonomic ganglia communicate with multiple organs to ultimately regulate cardiac functions to maintain hemodynamic homeostasis in traumatic brain injury (Goldberger et al., 2019). Understanding the functions of a crosstalk between the autonomic nervous system and heart in normal and disease conditions are keys to this research. Many cardiological studies have been undertaken to find out the involvement of autonomic neuronal dysfunction in many disease conditions such as arrhythmia, and sudden cardiac death. The clinical intervention to target the modulation of cardiac autonomic dysfunction is critical in improving the patient prognosis (Qin et al., 2019).

1.2.1. Anatomy and functions of the cardiac ANS

Anatomical structures on cardiac ANS are complex and there are two systems, i.e., sympathetic and parasympathetic. The cardiac nerves connecting to the cardiac plexus or distributing to the heart are named according to their origins as follows (Fountaine, 2018). Superior cardiac nerve is the cardiac nerve originating from the superior cervical ganglion or sympathetic chain. Thoracic cardiac nerve is the cardiac nerve originating from the thoracic stellate ganglia or the thoracic sympathetic chain below inferior cervical ganglion. Paravertebral sympathetic ganglion communicates with spinal nerves to control the heart innervated organs accordingly (Goldberger et al., 2019). The intrinsic cardiac ganglia is located in the epicardial muscle layer of the heart and it has both post-ganglionic sympathetic and pre-ganglionic parasympathetic nervous innervations. The balance of sympathetic and parasympathetic activities of heart are critical in regulating the physiological functions.

1.2.2. Arterial baroreflex circuitry

The arterial baroreflex is the most important mechanism for controlling of arterial blood pressure. The baroreceptor senses the fluctuations of blood pressure that occur in everyday situation. On the other hand, the reflex mechanisms regulate blood pressure in response to inputs from peripheral cardiovascular, respiratory, vestibular, and other receptors. The arterial baroreflex is a critical cardiovascular reflex that continuously modulate any

fluctuations in the blood pressure in normal and abnormal conditions of the body (Fountaine, 2018). The baroreflex controls cardiac output and total peripheral resistance to resultantly regulate blood pressure. For example, the activation of the baroreceptors after an increase in blood pressure results in suppressing the activities of sympathetic nerves innervating the heart and vessels, while increasing the parasympathetic activities of vagal output to the heart (i.e., the sinoatrial node). This results in decreases in cardiac output (CO) and total peripheral resistance (TPR) and then, blood pressure. In the conditions with low blood pressure, reduced baroreceptor activity causes the activation of reflex sympathetic circuit to increase CO and TPR

1.2.3. Arterial baroreceptor neurons

The arterial baroreceptor neuronal terminals are located in the carotid sinuses and aortic arch. These are mechanosensitive so the vessel dilatation or constriction will trigger off the baroreceptor afferent depolarization. There are several mechanosensitive channels in the baroreceptor afferents involves such as epithelial sodium channels (ENaCs), acid-sensing channels (ASIC), and transient receptor potential (TRP) channels and is regulated by several potassium currents and local signals (Snitsarev et al., 2007). Primary baroreceptor afferents provide excitatory input to neurons located in the nucleus of the solitary tract (NTS) (Blessing, 2003). Barosensitive NTS neurons initiate a sympathetic pathway which controls total peripheral resistance and heart rate.

The baroreflex's sympathetic pathway involves a projection from the NTS to send an inhibitory projection to sympathoexcitatory neurons located in the rostral ventrolateral medulla (RVLM) (Fig. 3). RVLM neurons pass on the excitatory signals to preganglionic neurons of the intermediolateral cell column and activate the sympathetic vasoconstrictor output to muscle, mesenteric, and renal blood vessels. This RVLM pathway is crucial for sustaining reflex control of blood pressure (Dampney et al. 2003). The baroreflex receives neural information from the NTS to a group of vagal preganglionic neurons located in the nucleus ambiguus. These cholinergic neurons project to the cardiac ganglion neurons that inhibit the automatism of the sinus and provide a beat-to-beat control of the heart rate (Spyer, 1994). There is a continuous regulation of the baroreceptor reflex depending on many physiologic conditions. This baroreflex modulation contributes not only to the short-term but also to the long-term control of blood pressure.

The baroreflex controls the heart rate and its main mechanism is via its effects on the sympathetic vasoconstrictor neurons modulating total peripheral resistance. The efferent sympathetic component of the baroreflex is mediated by preganglionic sympathetic neurons that release acetylcholine, which acts via ganglion-type nicotinic receptors to switch on the excitation of noradrenergic neurons in the sympathetic ganglia innervating the resistance blood vessels. On the other hand, decreased baroreceptor activity triggers an activation of sympathetic vasoconstriction and an increase in peripheral resistance and venous return. The disruption of this system in the TBI individuals are shown to have dysregulated cardiac autonomic system with

disrupted BRS (McMahon, 2011). The BRS dysregulation results in the impairment and damage to the cardiac functions affected by abnormal automacity.

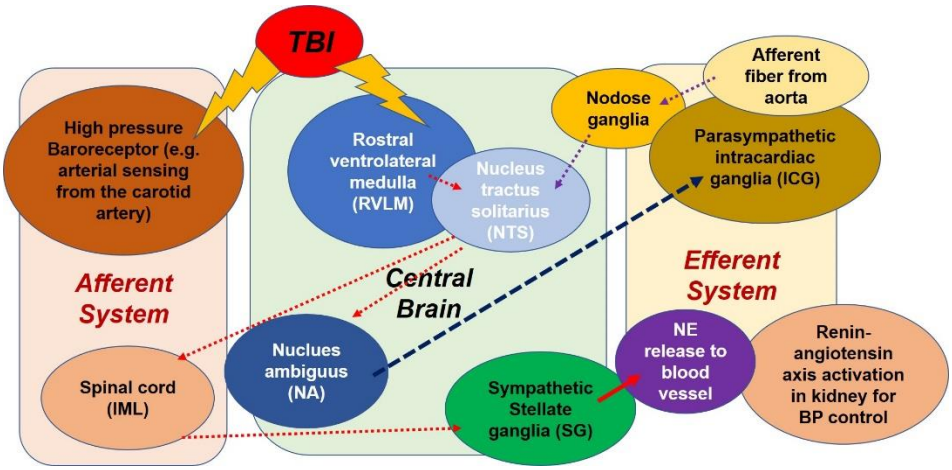

Figure 3. Schematic neural circuit of the arterial baroreflex. The circuit was consisted of sympathetic pathway from STG and parasympathetic flow of ICG, which was affected to heart rate and mean arterial pressure. If mean arterial pressure was increased, the negative feedback was started from the NG to the ICG via afferent and parasympathetic fiber.

1.2.3.1. Characteristics of arterial baroreceptor neuron subtypes

The aortic depressor nerve (ADN) is composed of both afferent A-fiber (about 25%) and C-fiber (about 75%) (Yamasaki et al. 2004). The sensory discharge characteristics are different between A-fiber and C-fiber baroreceptor afferents. C-fiber afferents are activated mainly at very high pressure and have lower firing frequencies with irregular discharge patterns (Thoren, Munch, and Brown 1999). The C-fiber afferents are known to be the primary regulators of tonic baseline levels of BP (Seagard et al. 1993). A-fiber afferents have lower pressure thresholds with very stable, proportional firing patterns (Thoren et al., 1999b). They are thought to regulate the baroreflex sensitivity but not baseline levels of BP (Seagard et al., 1993).

Electrophysiological and pharmacological examination of all these cells revealed that the AB neurons were comprised of two functionally distinct populations of A- and C-type AB neurons (Li et al., 2008). All A-type AB neurons are stimulated repetitively in response to the depolarizing step currents. In contrast, the unmyelinated C-type AB neurons exhibited very low discharge frequencies and often responded to step current magnitudes with short bursts of action potential discharges. Unlike myelinated A-type afferent neurons, all unmyelinated C-type afferent neurons exhibited a marked “hump” or delay over the repolarization phase of the somatic action potential waveform (Li and Schild 2007). A- and C-type AB neurons are pharmacologically identified based upon a differential sensitivity to the

selective ligand channel agonists capsaicin. (Li and Schild 2007) Recent reports demonstrated that the conduction velocities in A-type AB neurons did not respond to somatic application of capsaicin while the C-type AB neurons were capsaicin-sensitive (Reynolds et al., 2006a, Jin et al., 2004). Furthermore, the afferent synaptic transmission was blocked in the neurons within the NTS (Jin et al., 2004). In this respect, C-type AB neurons highly express TRPV1 channel in peripheral axons and in aortic arch terminations but A-type did not (Reynolds et al., 2006).

Voltage gated ion channels may involve in modulating arterial pressure and the neurotransmission of this information along the A- and C-type fiber pathways. Although various voltage-gated ion channels isoforms are expressed in both types, the relative expressions of each types of channels may form the unique discharge properties of the A-type and C-type baroreceptors (Schild and Kunze 2012).

The fast inward Na^+ current is a major determinant of the action potential threshold and the regenerative transmembrane current needed to sustain repetitive discharge (Schild et al., 2012). In the A-type baroreceptors the TTX-sensitive Nav1.7 channel contributes to the whole cell Na^+ current. However, NaV1.7 is lowly expressed in the C-type neurons in conjunction with TTX-insensitive NaV1.8 and NaV1.9 channels (Chen et al., 1997; Tu et al., 2010; Muroi et al., 2011). As a result, the action potentials of A-type neurons have firing thresholds that are 15-20 mV more negative with 5-10 times faster upstroke velocities when compared to the unmyelinated C-type neurons. A higher depolarized threshold of non-inactivating KV channel

subtypes produces C-type action potentials which are 3-4 times longer in duration than A-type neurons with low cellular excitability.

The C-type AB neurons also express KCa1.1 which comprises 25% of the total outward K^+ current. KCa1.1 plays a critically important role in shaping the action potential profile of C-type neurons while strongly influencing the neuronal excitability. The A-type AB neurons do not functionally express the KCa1.1 channel despite their whole cell CaV current is quite similar to that of C-type AB neurons (Li et al. 2008).

In both A- and C-type AB neurons the HCN current are activated at membrane potentials more negative than −50 mV. In the A-type AB neurons, the HCN channels are activated with nearly twice the firing rates and more than 10 times the magnitude of the HCN currents of the C-type neurons. The differences in the peak magnitude signifies the large contribution of HCN1 channels making the total HCN currents in the A-type AB neurons (Doan and Kunze 1999; Doan et al., 2004; Schild and Kunze, 2012). Interestingly, HCN2 and HCN4 expression levels are comparable in both types of AB neurons (Doan and Kunze 1999).

Together, such assembly of voltage gated ion channels strictly control the neural transmission of myelinated A-type baroreceptors to low threshold with high frequency but with a limited capacity for neuromodulation of afferent bandwidth. Unmyelinated C-type baroreceptors require greater depolarizing forces for activation, and usually have a low frequency discharge profile that is often poorly correlated with the physiological stimulus. However, the voltage gated ion channels in C-type neurons are more capable of

neuromodulation of cell excitability than the neurons from A-type baroreceptors. The resting membrane potential from different species ranges from approximately -60 mV. The variation in these values may reflect the species differences as well as sex and recording conditions such as methods.

Nevertheless, the molecular mechanisms of arterial baroreceptor is yet poorly understood. Recent evidence suggested that these mechanosensitive channels are epithelial Na^+ channels (ENaCs), acid-sensing ion channels (ASICs), and transient receptor potential (TRP) channels by pharmacological and genetic approaches (Drummond et al., 2008). The identification of the degenerin (DEG) / epithelial Na+ channel (ENaC) proteins has provided insight into the identity of mechanosensitive ion-channel complexes. These proteins are expressed predominantly in neuronal tissue and may play a role in mechanical sensation. They seem to have crucial roles in the kidney, colon, and lung epithelia as αENaC, βENaC, and γENaC form a heteromultimeric channel critical in Na^+ and water transport (Canessa et al., 1993). Most DEG/ENaC proteins form amiloride-sensitive, non-voltage-gated cation channels (Mcdonald and Welsh 1995). The mammalian epithelial Na^+-channel (ENaC) subunits have been reported to contribute to baroreceptor neurons (Drummond et al., 2001). The acid-sensing ion channel (ASIC) is a member of the DEG/ENaC family and is highly expressed in the mammalian central and peripheral nervous systems (Duggan et al., 2002). It has also been reported that the ion channels (ASIC2) play an important role in maintaining the integrity of the arterial baroreceptor reflex and the sensitivity of the baroreceptor neurons (Tan et al., 2010).

1.2.3.2. Functional roles of different Ion channels in cardiac afferent and efferent neurons

Sodium channels. Voltage-gated sodium channels (NaV) are important in the initiation and conduction of action potentials in excitable tissues and neural cells. TTX-sensitive NaVs currents are dominant in autonomic ganglion neurons. On contrary, mammalian primary afferent NG neurons (Ikeda and Schofield 1987) exhibit both TTX-sensitive and resistant NaV currents. Molecular studies have reported that there are nine specific NaVs α-chain subtypes (NaV1.1 to NaV1.9), and most of those except the NaV1.4 subtype have been found in sensory neurons (Liu and Wood 2011). Among them, NaV1.5, NaV1.8 and NaV1.9 are known to be TTX-resistant (TTX-R) (Catterall et al., 2005). Each subtype has unique kinetic properties in the generation of action potentials. The overall NaV current in many sensory neurons is biphasic showing a rapid activation and inactivation current followed by a slowly activating and inactivating current. (Caffrey et al., 1992).

Calcium channels. Voltage-gated Ca^{2+} (CaV) channels contribute to the electrical excitability, transmitter release, and gene expression in many types of neurons (Hille, 1992). CaV channels are involved in modulating membrane potential changes into intracellular Ca^{2+} transients that can act as secondary messengers to begin various physiological events. There are ten members of the CaV channel in mammals with different cellular functions. The CaV1

subfamily (L-type, CaV1.1 to 1.4) initiates contraction, secretion, gene expression, integration of synaptic input in neurons, and synaptic transmission at ribbon synapses in specialized sensory cells. The CaV2 subfamily (N-type, CaV2.1; P/Q-type, CaV2.2; R-type, CaV2.3) is primarily responsible for initiation of synaptic transmission at fast synapses (McCarthy and TanPiengco, 1992; Tsien et al., 1988; Dunlap et al., 1995; Catterall and Few, 2008). The CaV3 subfamily (T-type, CaV3.1 to 3.2) is important for repetitive firing of action potentials in rhythmically firing cells such as cardiac myocytes and thalamic neurons (Mangoni et al. 2006).

Potassium channels. So far, seven distinct voltage-activated K^+ currents have been identified in mammalian autonomic neurons: 1) a delayed outward rectifying K^+ channels; 2) a transient outward K^+ channels (A-channel); 3) Ca^{2+}-activated K^+ channels (BK- and SK-channels); 4) an inwardly rectifying K^+ channels; and 5) a muscarine-sensitive outward K^+ channel (KCNQ or M-Channel) (Adams et al., 1982).

Delayed outward rectifying K^+ channels are common in autonomic neurons and functions to repolarization of the action potential. The K^+ current turns on with a brief delay following the onset of membrane depolarization and persists while the depolarization is maintained (Sun et al., 2015). The transient outward K^+ (IA) channels are activated during the neuronal excitation, and functions to reduce the excitatory effects of depolarizing stimuli on a time-dependent manner. These channels contributed to the neuronal firing rate over a range of stimulus strength of synaptic transmission

(Daut, 1973) and afterhyperpolarization. Type IA is expressed in mammalian sympathetic neurons and regulates low-frequency repetitive discharge (Schofield and Ikeda 1989). Ca^{2+}-activated K^+ (KCa) channels are another key regulator of neuronal excitability, inter-spike interval and spike-frequency adaptation. Large conductance KCa (BK) channels show a very high single-channel conductance (-250 pS in symmetric 0.1 M KCl) and are activated by membrane depolarization and increases in intracellular $[Ca^{2+}]_i$. They play a role as feedback modulators of the activity of voltage-dependent calcium channels (VDCCs). Small conductance KCa (SK) channels play another major role in all excitable cells and are activated by an increased intracellular $[Ca^{2+}]_i$. The activation of SK channels causes membrane hyperpolarization inhibiting action potential firing. The intracellular $[Ca^{2+}]_i$ increase evoked by action potential firing decays slowly while SK channel are activated to generate a long-lasting hyperpolarization, i.e. slow afterhyperpolarization (sAHP) (Vergara et al. 1998). The KCNQ potassium channel gene family has three members: KCNQ1, KCNQ2, and KCNQ3 (Singh et al. 1998). The KCNQ2 and KCNQ3 subunits contribute to the M-current in central nervous system. KCNQ channel is activated in a voltage range between the resting potential and threshold (from -70 to -30 mV). KCNQ channels contribute to the normal resting membrane current and affects the general level of excitability (Shimizu et al., 1994).

Hyperpolarization-activated cation (HCN) channels. Four HCN isoforms (HCN 1–4) have been identified (Ludwig et al., 1999). These

isoforms exhibit 80–90% structural consensus in their core transmembrane regions and cyclic nucleotide binding domains (Santoro et al., 1999). All isoforms have been shown to form homomeric, hyperpolarisation-activated, non-selective cation channels that are directly modulated by cAMP in many different cells (Santoro et al., 1999). HCN channels are known to be activated during the afterhyperpolarization (AHP) of the action potential. HCN can act to depolarize the membrane, limit, and shorten the AHP, and promote multiple firings (Adams, 1995).

1.2.4. Ionic mechanisms underlying the excitability of intracardiac ganglion (ICG) neurons

The action potential and the different firing patterns in intracardiac neurons contributed to the regulation of blood pressure in the mammalian heart (Xi et al., 1991). The TTX sensitivity of the voltage-activated Na^+ current in rat parasympathetic neurons (Franklin et al., 1993) is known to be similar to the TTC sensitivity in rat sympathetic neurons (Schofield et al., 1988).

The components of the voltage-gated Ca^{2+} channels were N-type (63%), L-type (11%), and Q-type (19%), which were sensitive to ω-conotoxin GVIA, nifedipine, and ω-conotoxin MVIIC (Jeong et al., 1997), respectively. The electrical currents blocked with cocktail antagonists represent the R-type current (7%), which was sensitive to 100 μM $NiCl_2$ (Jeong et al., 1997).

Meanwhile, the muscarine-sensitive K^+ current, M-current, regulates the discharge activity in neonatal rat ICG neurons. Whereas the Ca^{2+}-activated

K^+ current blockers such as charybdotoxin and apamin had no effect on firing frequency (Cuevas et al., 1997). The Ca^{2+}-activated K^+ current is known to form approximately 35% of the total outward K^+ current observed in rat parasympathetic cardiac neurons. The Ca^{2+}-activated K^+ current in rat parasympathetic cardiac neurons contributes to the AHP (Xu and Adams 1992) which is disappeared by the removal of extracellular Ca^{2+} or addition of Cd^{2+} to the extracellular solution in cultured ICG neurons of the guinea-pig (Allen et al., 1987).

The Cd^{2+}-resistant delayed rectifier K^+ current in rat parasympathetic neurons contributes to maintaining the resting membrane potential, and to the repolarization phase of the action potential (Xu et al., 1992). The transient-outward (A-current) and inwardly rectifying K^+ currents have been described in rat sympathetic neurons. However, they were not detectable in cultured rat parasympathetic cardiac neurons (Belluzzi et al., 1985).

1.2.5. Ionic mechanisms underlying the excitability of stellate ganglion (SG) neurons

The electrophysiological properties and modulation of SG neurons by neuroactive agents are yet poorly understood whereas the autonomic neurons from paravertebral superior cervical ganglion (SCG) (Shapiro et al., 1994) and enteric ganglion (Adams, 1995; Vanner et al., 1993) are better studied.

The enzymatic dissociated SG neurons in adult rats (Tu et al., 2014) were

exhibited spontaneous action potentials (Gilbert et al. 1998). The major components (85–90%) of voltage-gated Ca^{2+} currents are dihydropyridine-insensitive, N-type Ca^{2+} channels (Plummer et al., 1989) in the mammalian sympathetic neurons, which was experimentally confirmed by complete blockade (95% of the Ca^{2+} current) by ω-conotoxin.

The outward current of K^+ and several voltage-dependent K^+ conductance was identified on the basis of voltage dependence and pharmacological blockade and consisted of a transient outward K^+ conductance, resembling A-type conductance described in mammalian autonomic neurons, (Belluzzi et al., 1985), and a delayed rectifier K^+ current consisting of Ca^{2+}-activated and Ca^{2+}-insensitive components (Gilbert et al. 1998).

1.3. Cardiac autonomic dysfunction (CAD)

As mentioned earlier, the ANS is crucial in maintaining the physiological homeostasis. The wide network of ANS is susceptible to the injury and the disruption in the system can occur by many diseases such as TBI, stroke, primary hypertension, diabetes mellitus, and auto-immune diseases (Goldberger et al., 2019). Patients with cardiac autonomic dysfunction (CAD) show impaired baroreflex in the cardiac or peripheral innervating network. This may play a critical role in disrupting the hemodynamic outcome during the disease processes as well as cardiovascular manifestations to dysregulate autonomic system.

1.4. Relationship of TBI and CAD

TBI causes the uncoupling of the autonomic nervous system from the heart during the post-injury period. There are evidences of altered cardiovascular regulation after acute traumatic brain injury (TBI) (Pearn et al., 2019). The loss of a normal autonomic control in the heart is known to frequently occur after moderate to severe TBI (Henden et al., 2014) The presence of CAD is specifically associated with an increased morbidity and mortality and can be used to predict the risk of progression to brain death. (Henden et al. 2014)

The onset and progression of TBI-induced CAD is manifested by a loss of normal heart rate variability (HRV) and a blunted baroreflex sensitivity (BRS), which reflects an imbalance between the sympathetic and parasympathetic influences on the heart (Keren et al., 2005). Currently, however, there is a lack of preclinical studies that reproduce the characteristics of the CAD observed in TBI patients. Importantly, the cellular mechanisms underlying TBI-induced CAD remain unsolved. Theoretically, TBI-induced CAD may arise from profound structural and functional defects in the central and peripheral neural components that mediate the autonomic regulation of the heart. In the present study, we hypothesized that TBI-induced CAD is associated with functional plasticity in cardiac efferent neurons. Thus, we examined whether the excitability of sympathetic stellate ganglion (SG) and parasympathetic intracardiac ganglion (ICG) neurons is altered, and the consequent ionic mechanisms that underlie the dysfunction of the cardiac efferent neurons in an experimentally-induced rat model of TBI.

For instance, in severe TBI with severe stress hormone release, hyperadrenergic condition leads to abnormal sympathetic hyperactivity that it eventually results in the damages to the heart muscles (Clifton et al., 1983). Neurocritical care involves both neurosurgical emergency care as well as stable cardiovascular and respiratory management after TBI to minimize secondary injuries so that the cerebral perfusion is sustained until the patient is recovered (Khalid et al., 2019).

II. PURPOSES

2.1. Rationale and hypothesis

Traumatic brain injury (TBI) frequently causes cardiac autonomic dysfunction (CAD), irrespective of its severity, which is associated with an increased morbidity and mortality in patients. Clinically, the onset and progression of TBI-induced CAD is manifested by a loss of normal heart rate variability (HRV) and a blunted baroreflex sensitivity (BRS), which reflects an imbalance between the sympathetic and parasympathetic influences on the heart. Currently, however, there is a lack of preclinical studies that reproduce the characteristics of the CAD observed in TBI patients. Importantly, the cellular mechanisms underlying TBI-induced CAD remain unsolved. Accordingly, the working hypothesis in the present study is that TBI-induced CAD is associated with functional plasticity in the cardiac efferent and afferent neurons.

2.2. Purposes

I. To examine whether TBI causes CAD in rats.

(1) To validate whether the TBI rat models are suitable for studying the cellular mechanisms underlying CAD.

(2) To examine whether BRS and HRV are reduced in TBI rats

II. To examine whether TBI induced functional plasticity of rat cardiac efferent and afferent neurons.

(1) To examine whether the cell excitability is altered in the SG and ICG neurons from TBI rats

(2) To define the ionic mechanisms underlying the functional plasticity of the cardiac efferent neurons

(3) To examine whether the cell excitability is changed in the A- and C-type AB neurons from TBI rats

III. MATERIALS AND METHODS

3.1. List of chemicals and stock concentration

Capsaicin (Sigma-Aldrich, St. Louis, MO, USA), 1 mM

Formaldehyde (Duksan, Ansan, Korea), 4%

Isoflurane (Terrell, Minrad Inc., Bethlehem, PA, USA)

Penicillin–streptomycin solution (Hyclone, Logan, UT, USA) 1%

Phenylephrine (PE, Sigma-Aldrich), 40 mg/ml

Surgicel® (Johnson & Johnson, Arlington, TX, USA)

Urethane (Sigma-Aldrich), 1 g/ml

TTC solution (Sigma-Aldrich, St. Louis, MO, USA). 2%

3.2. Animals

Male Sprague-Dawley rats (8 week-old) were obtained from DBL Co. (Eumseong-Gun, Republic of Korea), and were randomly allocated into three groups: (i) sham (control) (*n = 15*); (ii) moderate TBI (mTBI) (*n = 15*), and (iii) severe TBI (sTBI) (*n = 15*) groups. The rats were housed in separate cages under controlled cycle of light and dark at 22℃ free access to food and drinks.

All animal care and experimental procedures were approved by the Institutional Animal Care and Use Committee of Yonsei University Wonju

College of Medicine (YWC-150408-1).

3.3. Controlled cortical impact (CCI) model of TBI

Anesthesia was administered using 4% isoflurane in an anesthesia induction chamber, followed by subsequent inhalation of 2% isoflurane inhalation through a rodent nasal cone during all surgical and impact procedures. Induction of deep anesthesia was confirmed by testing the pain reflex, and then each rat was placed in a stereotaxic frame (David Kopf Instruments, Tujunga, CA, USA) attached to a TBI-0310® head impactor device (Precision Systems & Instrumentation, Fairfax Station, VA, USA), as previously described (Khan et al., 2009) (Fig. 5). The ears of the rats were fixed, so that the head was positioned in parallel with the base plate by the nose bar. And then, a linear incision of 3 cm is performed in the midline of the brain scalp. After retracting the scalp, the periosteal membrane is denuded to reveal coronal suture with bregma. After exposing the skull, a craniotomy was performed by making a burr hole of 6 mm in diameter, 1 mm posterior to the coronal suture at the level of the left parietal cortex using an IPC® surgical drill (Medtronic, Forth Worth, TX, USA). Care was taken to avoid any injury to the dura, parenchymal structure and vascular structures. The impacting rod with a 5 mm tip was positioned at a right angle to the cortical surface of the left parietal lobe. A single CCI (4-m/s of velocity and 200 ms of dwell time) was delivered with a contusion depth of either 2.5 mm (for the moderateTBI (mTBI) group) or 4 mm (for the severe TBI (sTBI) group).

Any mild bleeding after brain contusion was controlled using Surgicel® (Johnson & Johnson, Arlington, TX, USA) and then, the scalp wound was closed using surgical staples. The sham group underwent all surgical procedures, except CCI delivery. A rectal temperature around 37°C was maintained using a heating pad and a manually controlled lamp during the experiments. All animals were allowed to recover from anesthesia and to return to their cages. The overall design of the experiment is depicted in Fig. 4.

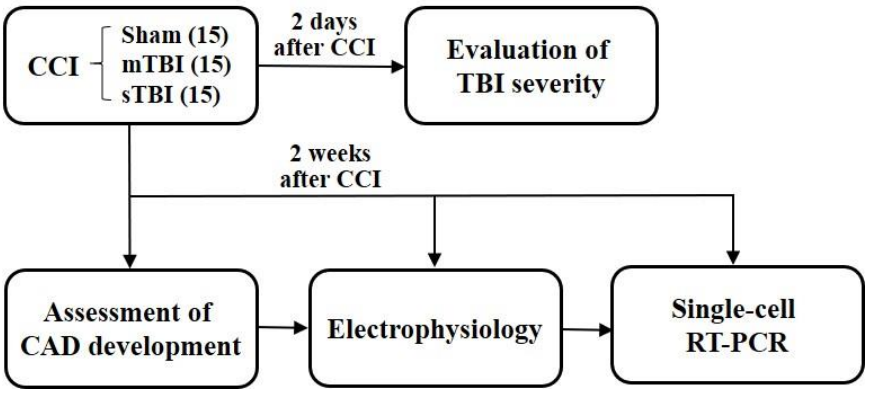

Figure 4. The design of experimental procedure. Rats were divided into three groups: sham-control (n = 15), mild TBI (mTBI) (n = 15), and severe TBI (sTBI) (n = 15). The degree of TBI severity was controlled by the contusion depth of controlled cortical impact (CCI). Two days after CCI, the cortical lesion volume was measured after TTC staining to validate the degree of severity (n = 5 /group). Two weeks after CCI, CAD development was assessed by measurement of HRV and BRS (n = 5 /group). After then, electrophysiological recordings and single-cell RT-PCR were performed.

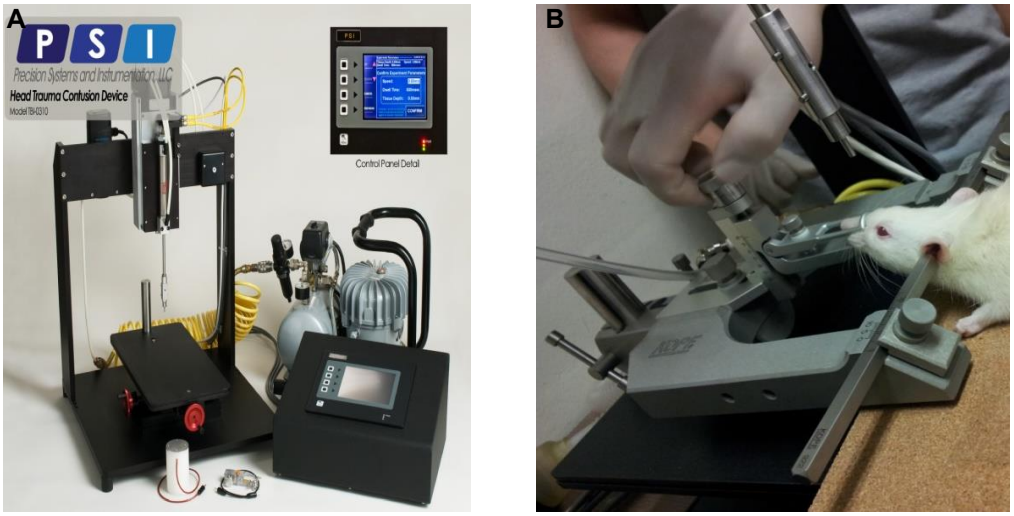

Figure 5. Controlled cortical impact (CCI) model. Head impactor device (A) and Head fixation with stereotaxic frame (B). Induction of deep anesthesia was confirmed by testing the pain reflex, and then each rat was placed in a stereotaxic frame (David Kopf Instruments, Tujunga, CA, USA) attached to a TBI-0310® head impactor device (Precision Systems & Instrumentation, Fairfax Station, VA, USA).

Table 1. The controlled cortical impact parameters for different TBI severity

Severity of head injury	Velocity (m/sec)	Indwell time (msec)	Depth (mm)
Control	0	0	0
Moderate	4	200	2.5
Severe	4	200	4

3.4. Evaluation of TBI-induced cortical lesion volume

Two days after CCI, the cortical lesion was visualized using 2,3,5-triphenyltetrazolium chloride (TTC) staining (Bederson et al. 1986). Briefly, rats were anesthetized with sodium thiopental (100 mg/kg) and decapitated. The brains were quickly removed and placed in a chilled saline solution. After assessment of the macroscopic lesion of the cortical surface, serial 2-mm-thick coronal slices were rostro-caudally cut using a rodent brain slicer. The brain slices were immersed in a 2% TTC solution (Sigma, St. Louis, MO, USA) for 15 minutes at 37 °C and then, were fixed in 4% paraformaldehyde solution. Brain infarction was evident by a negative TTC staining due to the loss of various dehydrogenases. The cortical lesion volume in each slice was quantified using the NIH image analysis software (ImageJ 1.41, NIH, Bethesda, MD, USA) as previously described (Yu et al., 2009).

3.5. Power spectral analysis of heart rate variability (HRV)

Two weeks after CCI, ECG was recorded in rats under anesthesia with 2% isoflurane (Murakami et al., 2014). Three electrodes were implanted subcutaneously to record the apex-base lead ECG (Gao X Y et al., 2011). The electrodes were connected to a Bio amplifier (AD Instruments, Colorado Springs, CO, USA) with signals digitized through an A/D converter Power Lab system (AD Instruments) (Fig. 6). The digitized ECG data were analyzed using Lab Chart v7 software (AD Instruments). Spectral density power of the

various frequency components from cycle length variability was calculated using the fast Fourier transform algorithm. Low frequency (LF) and high frequency (HF) components were distinguished in a spectrum calculated from short-term recordings of 2 minutes. LF and HF powers were defined as the area under the curve in the frequency range of 0.04-1.0 Hz and 1.0-3.0 Hz, respectively (Hashimoto et al. 1999). The ratio between the LF and HF components (LF/HF ratio) was calculated to evaluate the balance between sympathetic and parasympathetic activities (Malliani et al., 1991).

3.6. Evaluation of the arterial baroreflex

The arterial baroreflex was evaluated by measuring the slowing of the heart rate (HR) in response to an increase in the blood pressure induced by injection of phenylephrine (PE) (Lee et al., 2016). Briefly, sham and TBI rats were anesthetized with urethane (0.75g/kg in 0.9% saline, intraperitoneally (i.p.)). The a thin cannula is inserted into the right femoral artery to record the blood pressure and HR. The left femoral vein was also cannulated to administer PE or saline. The arterial pressure and HR were synchronously and continuously recorded using a Power Lab data acquisition system and LabChart v7 software (AD Instruments). After a 10 minute stabilization period, the peak increases in the mean arterial pressure (MAP) in response to PE (5, 10, 20, and 40 mg/kg), and the associated peak reflex decreases in the HR were recorded. (Fig. 6) The HR changes were converted to pulse interval (PI, ms) values using the following formula: 60,000/HR. For each drug dose, the

BRS was calculated as the ratio between changes in the HR (as PI) and changes in MAP (ΔPI/ΔMAP, ms/mm Hg). The BRS was also determined for each rat as the slope (gain) of the relationship between ΔPI and ΔMAP in the range of all PE doses.

Figure 6. Measuring baroreflex. After ECG application, the femoral artery and vein access were ontained and the information from the power spectral analysis were recorded from the transducer inserted in the femoral artery. The femoral vein is punctured with catheter for drug application. Via an injector, the vasopressor drugs were given and the BRS were measured via arterial transducer connected to the PowerLab and LabChart program.

3.7. Dissociation of cardiac efferent neurons

The SG and ICG neurons were enzymatically dissociated as previously described (Jeong et al. 1999). The ganglion is isolated in cold HBSS buffer (pH 7.4) and incubated in the enzyme cocktails containing collagenase (1 mg/mg, trypsin 0.3 mg/ml, and DNaseI 0.1 mg/ml) for 1 hour in the shaking water bath at 37°C. The dissociated neurons were washed two times and suspended in Minimum Essential Medium containing 10% fetal bovine serum and a 1% penicillin–streptomycin solution (all from Roche). Neurons were then plated onto poly-D-Lysine coated culture dishes (35 mm) and maintained in a humidified atmosphere of mixed gases containing 95% air and 5% CO_2 at 37°C.

3.8. Di-I labeling of aortic baroreceptor (AB) neurons.

The retrograde neuronal tracer, Di-I (1,1-didodecyl-3,3,3,3-tetramethylindocarbo-cyanine perchlorate, 0.25% in DMSO) (Molecular Probes, Eugene, OR) was used to identify AB neurons that projected to the aorta as previously described. One or two weeks prior to the electrophysiological recording, the rats were anesthetized with 2% isoflurane and mechanically ventilated. After a thoracotomy at the third intercostal space, the aortic arch was exposed after the retraction of pulmonary artery. Approximately 2 μL of Di-I was injected into a part of the adventitia of the aortic arch with a microinjector. After the injection of Di-I, the surgical incision was closed, negative intrathoracic pressure was re-established, and the

animals were allowed to rest and recover. All surgical procedures were performed under sterile conditions.

3.9 Dissociation of cardiac afferent neurons

Single nodose ganglion neurons were enzymatically dissociated as previously described (Lee et al., 2016). Briefly, adult male rats (200–300 g) were anesthetized with urethane (800mg/kg). A pair of nodose ganglia was dissected and placed in cold Hanks' balanced salt solution (pH 7.4). The ganglia were desheathed, cut into small pieces, and incubated with 1 mg/ml collagenase type D (Roche, Diagnostics, Germany), 0.15 mg/ml trypsin (Worthington. Corporation, Harrison, NJ), and 0.1 mg/ml DNase type I (Sigma, St Louis, MO) in modified Earle's balanced salt solution (EBSS, pH 7.4) in a 25-cm^2 tissue culture flask. The EBSS was modified by adding 3.6 g/L glucose (Sigma, St Louis, MO) and 10 mM HEPES (Sigma). The flask was then placed in a shaking water bath at 100 rpm and 35.5°C for 60 minutes. After incubation, the ganglia were dispersed into single neurons by vigorously shaking the flask containing the ganglia. After centrifugation at 1200 rpm for 3 minutes, the dissociated neurons were resuspended in minimum essential medium (MEM) (Invitrogen, CA) containing 10% fetal bovine serum (Invitrogen), L-glutamine (Invitrogen) and 1% penicillin-streptomycin (Hyclone, Logan). The neurons were then plated on to culture dishes (35 mm) coated with poly-L-lysine (Sigma) and maintained in a humidified 95 % air-5 % CO_2 incubator at 37 °C until use.

3.10. Electrophysiological recordings

Current-clamp and voltage-clamp recordings were performed under the gramicidin-perforated and whole-cell-ruptured configurations of the patch-clamp technique, respectively, using an EPC-10 amplifier and pulse/pulsefit (v8.50) software (HEKA Electronik, Lambrecht, Germany), as previously described (Lee et al., 2016; Won et al., 2006). For the current-clamp recordings, a normal physiological salt solution was used as the external solution and contained (in mM) 135.0 NaCl, 5.4 KCl, 10.0 HEPES, 10.0 glucose, 1.8 $CaCl_2$, and 1.0 $MgCl_26H_2O$ (pH 7.4, 318 mOsm/kgH_2O). A stock solution of gramicidin was prepared at a concentration of 50 mg/mL (in DMSO) and diluted (50 μg/mL final concentration) in an internal solution that contained (in mM): 20.0 KCl, 120.0 K-gluconate, and 10.0 HEPES (pH 7.2, 310 mOsmol/kgH_2O). To record the K^+ currents, the external solution contained (in mM): 150 Choline-Cl, 5 KCl, 10 HEPES, 1.5 $CaCl_2$, 5 $MgCl_2$, 0.2 $CdCl_2$, and 10 Glucose (pH 7.4, 325 mOsm/ kgH2O). Patch pipettes were filled with an internal solution containing (in mM): 140 KCl, 5 Ethylene-bis(oxyethylenenitrilo) tetraacetic acid (EGTA), 1 $MgCl_2$, 0.5 $CaCl_2$, 10 HEPES, 3 Mg-ATP, and 3 Na-GTP (pH 7.3, 310 mOsm/ KgH2O) for A-type and delayed rectifier K^+ currents, and 140 KCl, 0.1 1,2-Bis(2-aminophenoxy) ethane-N,N,N′,N′-tetraacetic acid (BAPTA), 10 HEPES, 4 Mg-ATP, and 0.1 Na-GTP (pH 7.4, 310 mOsm/Kg H_2O) for M-type K^+ currents. Patch electrodes were fabricated from a boroslicate glass capillary (#8250) (King Precision Glass, Inc., Claremont, CA, USA). The electrodes were coated with

Sylgard 184 (Dow Corning, Midland, ML, USA) and fire-polished on a microforge, to obtain a resistance of 2-3 MΩ, when filled with the internal solution described above. The cell membrane capacitance and series resistance were electronically compensated for over 80%. All experiments were performed at room temperature (24 °C).

3.11. Single-cell qPCR

Single-cell quantitative PCR (qPCR) was carried out as previously described with minor modifications (Liu et al. 2012). An enzymatically dissociated single neuron was pulled into a patch pipette under negative pressure. The pipette tip containing the single cell was broken into a 0.2-mL PCR tube containing the following reagents: 5 μL volume consisting of 1 μL of lysis buffer (0.25 M Tris·HCl, 0.275 M KCl, 0.015 M $MgCl_2$, and 2.5% Nonidet P-40), 0.5 μL of RNA guard Mix consisting of 1 μL of a 10X first-strand cDNA synthesis buffer from Sensiscript Reverse Transcripase Kit (Qiagen, Valencia, CA, USA), 2 μL of RNase inhibitor (Applied Biosystems, Foster City, CA, USA), and 7 μL of DEPC-treated water, and 3.5 μL of DEPC-treated water, and then kept at -80 °C until reverse transcription was performed. First-strand cDNA was synthesized from the 5 μL of each tube using Sensiscript Reverse Transcripase Kits (Qiagen) according to the manufacturer's instructions. The cDNA was then stored at −80°C until real-time PCR. The sequences of the single-cell qPCR primers are listed in Table 2. To increase the specificity and sensitivity of the PCR, we used outer pair

primers in first-round of PCR and inner pair (nested or semi-nested) primers in the second-round of PCR. In addition, the primers were designed to amplify the segments of cDNA that consisted of two or more exons to prevent genomic DNA amplification. PCR amplification was conducted using a 7900HT Fast Real-Time PCR System (Applied Biosystems). PCR reaction was performed in a 25 μL volume containing 12.5 μL of SYBR Green master mix (Applied Biosystems), 40 nM (in the first round) or 300 nM (in the second round) of each primer. In the first round of amplification, a 2 μL aliquot of the reverse transcription product was used and then 5 μL of the first-round product were used in the second round of amplification. After preheating at 94 °C for 10 min, the amplification was performed for 30 - 35 thermal cycles of 94°C for 15 s, 60 °C for 1 - 2 min and 72 °C for 2 min, and a final extension at 72 °C for 5 min. The β-actin gene was amplified as a house keeping gene for reference. The fold changes in gene expression were analyzed using the comparative $2^{-\Delta\Delta CT}$ Livak method (Livak et al., 2001).

Table 2. Single cell qPCR primer sequences

Target	Accession No.	Sequence (5'-3')	Size (bp)
β-actin	NM031144.2	F_{ext}: ACCAGTTCGCCATGGATGAC R_{ext}: GGTCTCAAACATGATCTGGG	389
		F_{int}: ATGGTGGGTATGGGTCAGAA R_{int}: ACCAACTGGGACGATATGGA	119
K_V 4.1	NM001105748.1	F_{ext}: CCGTATATACCACCAGAACC R_{ext}: GGAAGGTTGACTCTCATCTG	610
		F_{int}: TTGCCAACTCTACTGCGTC R_{int}: TTGGCATTGAGGCTTGAGC	109
K_V 4.2	NM031730.2	F_{ext}: GGTGATGACAGACAATGAGG R_{ext}: CACAAACTCATGGTTCGTGG	652
		F_{int}: ACAAACGAAGGGCACAGAAG R_{int}: AGTTGGTTGCTCAGTAACCC	109
K_V 4.3	NM031739.3	F_{ext}: CATCATCATCTTTGCCACTG R_{ext}: ATTAAGGCTGGAGCGACTAG	733
		F_{int}: TATTTGGCTCCATCTGCTCC R_{int}: TTCTTCTGTGCCCTGCGTTT	127
K_V 7.2	NM133322	F_{ext}: ACTGTCCCCATGATCAGCTC R_{ext}: TCTGATGCTGACTTTGAGGC	471
		F_{int}: GAGTCTCGATGACAGCCCAA R_{int}: AGGGAGGCTTGCTTCTTCTG	127
K_V 7.3	NM031597.3	F_{ext}: GCAATGTCCTGGCTACCTCT R_{ext}: TTTTGGCTGGCTGCTGCTTC	613
		F_{int}: CAGCAAAGAACTCATCACCG R_{int}: ACAGGGCATCAGCATAGGTC	152

(*ext: nested external primer; int: nested internal primers)

3.12. Data analysis and statistics

The electrophysiological data were analyzed using the IGOR data analysis package (Wave-Metrics, Lake Oswego, OR, USA) or GraphPad Prism (v4.0, GraphPad Software Inc., La Jolla, CA, USA).

The data are presented as the mean ± SEM. A Student's t-test or one-way ANOVA with a post-hoc test (Tukey's multiple comparison test) was performed. A value of $p < 0.05$ was considered statistically significant.

IV. RESULTS

4.1. Evaluation of CAD in rats with moderate and severe TBI

TBI was induced by CCI, which delivers a focal mechanical insult to the intact dura in rats. The degree of TBI severity was controlled by the contusion depth of CCI (Yu et al., 2009). Two days after CCI the cortical lesion was visualized using 2,3,5-triphenyltetrazolium chloride (TTC) staining for quantifying the cortical lesion volume (Bederson et al., 1986). As shown in Fig. 7, the cortical lesion volume was proportional to the severity of TBI. The control group had no detectable cortical lesions (Fig. 7A). On the other hand, the mTBI and sTBI groups exhibited a cortical lesion volume of 18% ± 1% (n = 5) and 37% ± 3% (n = 5), respectively (Fig. 7B), which was comparable to the previous study (Yu et al., 2009).

The development of CAD was assessed two weeks after TBI. Power spectral analysis of HRV showed that the total power (TF) and HF were significantly decreased ($p < 0.001$), and LF tended to decrease, but not significantly, in the mTBI ($p = 0.413$) and sTBI ($p = 0.326$) groups, compared with the control group (Table 3). On average, TF, LF, and HF (in ms^2) were 12.1 ± 1.67, 1.21 ± 0.28, 3.45 ± 0.53 in the control group (n = 5), 6.3 ± 1.23, 0.82 ± 0.18, 1.01 ± 0.2 in the mTBI group (n = 5), and 4.5 ± 0.87, 0.85 ± 0.2, 0.72 ± 0.21 in the sTBI group (n = 5), respectively. Importantly, In the mTBI ($p < 0.01$) and sTBI ($p < 0.001$) groups, the LF/HF ratio was significantly increased, which suggests an autonomic imbalance with excessive sympathetic activity and a reduced parasympathetic activity (Table 3). On

average, the LF/HF ratio was 0.35 ± 0.07, 0.81 ± 0.08, and 1.18 ± 0.13, respectively in the control, mTBI, and sTBI groups, respectively.

To investigate the impaired arterial baroreflex in the TBI groups, we assessed the BRS by measuring the peak increases in the MAP to PE (5, 10, 20, and 40 mg/kg) and the associated peak reflex decreases in the pulse rate. As shown in Fig. 8A, the BRS (ΔPI/ΔMAP, ms/mm Hg) for each drug dose was significantly lower in the mTBI ($n = 5$, $p < 0.05$ for PE5, $p < 0.01$ for PE10, and $p < 0.001$ for PE20 and PE40) and sTBI ($n = 5$, $p < 0.05$ for PE10, and $p < 0.001$ for PE20 and PE40) groups, than in the control group ($n = 6$). The baroreflex gain, the slope of the relationship between ΔPI and ΔMAP was significantly lower in the mTBI (0.45 ± 0.09, $n = 5$, $p < 0.01$) and sTBI (0.47 ± 0.08, $n = 5$, $p < 0.01$) groups, compared to the control group (0.98 ± 0.08, $n = 5$) (Fig. 8B). In summary, these data indicate that the arterial baroreflex is impaired in TBI rats regardless of the severity.

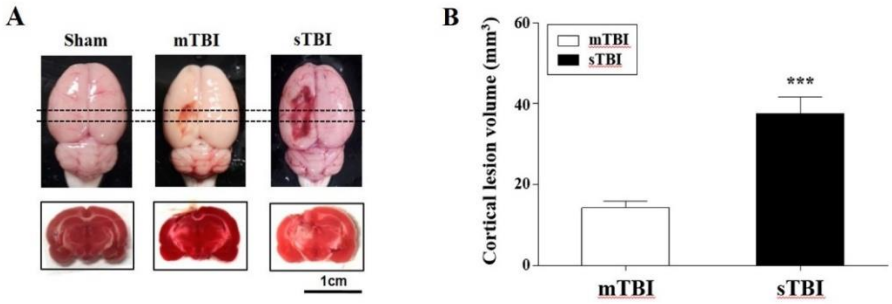

Figure 7. Cortical lesion volume along to the TBI classification. (A) Histologic assessment of the cortical lesion volumes measured after mTBI and sTBI in rats, gross findings of the cortical lesion by CCI (upper) and TTC staining of each brain slice (lower). **(B)** The cortical lesion volume (%) in rats with mTBI and sTBI. The cortical lesion volume in each slice was quantified using the NIH image analysis software. Data are presented as the mean ± SEM. ***P < 0.001 compared to the sham group.

Table 3. Summary of HRV for sham (control), mTBI, and sTBI groups

HRV Variables	TP (ms^2)	VLF (ms^2)	LF (ms^2)	HF (ms^2)	LF/HF
Sham	12.1 ± 1.67	7.41 ± 2.12	1.21 ± 0.28	3.45 ± 0.53	0.35 ± 0.07
mTBI	6.3 ± 1.23*	4.67 ± 1.25	0.82 ± 0.18	1.01 ± 0.2**	0.81 ± 0.08**
sTBI	4.5 ± 0.87**	3.01 ± 0.41**	0.85 ± 0.2	0.72 ± 0.21***	1.18 ± 0.13***

Data are presented as the mean ± SEM.

*P < 0.05, **P < 0.01, ***P < 0.001 compared with the sham group.

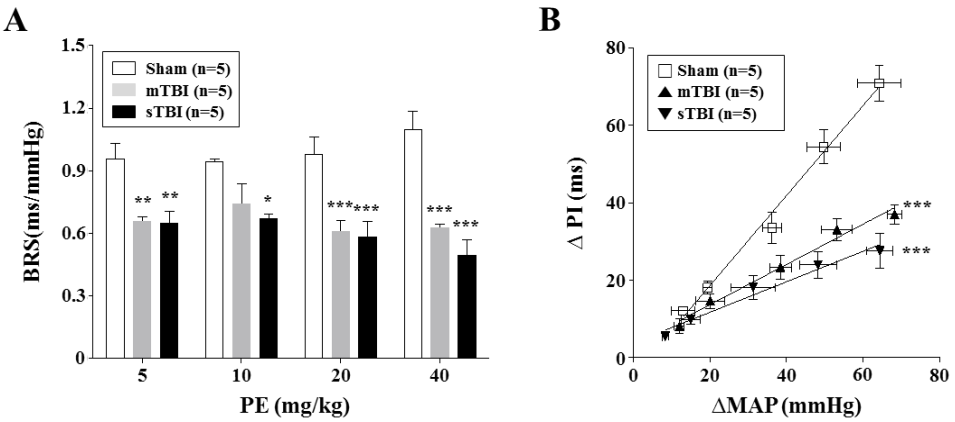

Figure 8. Assessment of the arterial baroreflex in the sham (control), mTBI, and sTBI groups. (A) summary of the BRS for different doses of PE (5, 10, 20, and 40 mg/kg), **(B)** comparison of the slope of the relationship between the △PI and △MAP. Data are presented as the mean ± SEM. ###P <0.001 compared between the mTBI and sTBI groups; *P < 0.05, **P < 0.01, ***P < 0.001 compared with the sham group.

4.2. Alterations in the cell excitability of cardiac efferent neurons from the TBI groups

Sympathetic SG and parasympathetic ICG neurons were found to innervate the heart (Wallis et al., 1996). We examined whether the autonomic imbalance observed in TBI rats is associated with alterations in the excitability of these cardiac efferent neurons. Consistent with a previous study (Tu et al., 2014), all the tested SG and ICG neurons in the control group exhibited a regular discharge of action potential (AP) in response to a depolarizing current injection for 1 second under the gramicidin-perforated configuration of the patch-clamp technique (Fig. 9). The excitability in the SG neurons of TBI groups was significantly increased compared with the control group ($p < 0.001$ for the control group vs. the mTBI group and $p < 0.001$ for the control group vs. the sTBI group) (Fig. 9A & 9B). In contrast, the excitability of the ICG neurons in the TBI groups was significantly decreased when compared with the control group ($p < 0.001$ for the control group vs. the mTBI group, and $p<0.001$ for the control group vs. the sTBI group) (Fig. 9C & 9D). The SG neurons of the control group (n = 13) discharged at 4.2 ± 0.4, 6.5 ± 0.4, and 8.6 ± 0.5 spikes/s in response to 1X, 2X, and 3X threshold current stimulations, respectively. The SG neurons of the mTBI group (n = 12) discharged at 6.5 ± 0.3, 9.8 ± 0.5, and 12.0 ± 0.6 spikes/s, and the SG neurons of the sTBI group (n = 14) discharged at 7.4 ± 0.3, 10.5 ± 0.4, and 13.0 ± 0.4 spikes/s, in response to 1X, 2X, and 3X threshold current stimulations, respectively. The ICG neurons of the control group (n = 10)

discharged at 5.7 ± 0.4, 8.0 ± 0.5, and 11.0 ± 0.6 spikes/s in response to 1X, 2X, and 3X threshold current stimulations, respectively. The ICG neurons of the mTBI group (n = 12) discharged at 2.6 ± 0.5, 4.6 ± 0.5, and 6.6 ± 0.5 spikes/s, and the ICG neurons of the sTBI group (n = 13) discharged at 2.0 ± 0.3, 4.0 ± 0.7, and 5.8 ± 0.6 spikes/s in response to 1X, 2X, and 3X threshold current stimulations, respectively. There was no significant difference in the number of discharges between the two TBI groups. Taken together, these data suggest that TBI causes the hyperexcitability of sympathetic cardiac neurons and the hypoexcitability of parasympathetic cardiac neurons.

The altered excitability in the cardiac efferent neurons of the TBI groups was also assessed by measuring the threshold potential and rheobase for triggering AP. Thus, the SG and ICG neurons were stimulated with an increasing depolarizing current injection for 5 ms, until a single AP was generated (data not shown). Compared with the control group, the two measures of excitability were significantly decreased in the SG neurons of the TBI groups ($p < 0.05$) (Table 4). On average, the threshold potentials were -31 ± 0.7 mV (n = 13), -37.1 ± 1.1 mV (n = 12), and -38.3 ± 1.5 mV (n = 14), respectively, in the SG neurons of the control, mTBI, and sTBI groups. Rheobase was 63 ± 5 pA (n = 13), 43 ± 5 pA (n = 12), and 40 ± 5 pA (n = 14), respectively, in the SG neurons of the control, mTBI, and sTBI groups. Conversely, the threshold potential was significantly increased in the ICG neurons of the TBI groups ($p < 0.05$) compared with the control group (Table 4). On average, the threshold potentials were -31.7 ± 1.0 mV (n = 10), -23.7

± 1.5 mV (n = 12), and -21.2 ± 2.0 mV (n=13) in the SG neurons of the control, mTBI, and sTBI groups, respectively. In accordance with the changes in the threshold potential, the rheobase was significantly increased in the ICG neurons of the mTBI group (81 ± 4 pA, n = 12, $p < 0.05$) and sTBI group (87 ± 5 pA, n = 13, $p < 0.05$) compared with the control group (72 ± 6 pA, n = 10).

Other electrical properties of the SG and ICG neurons were also compared between the control and TBI groups (Table 4). The AP duration (at 0 mV) was significantly altered in the SG and ICG neurons of the TBI groups when compared with the control group ($p < 0.05$). On the other hand, TBI effects on cell capacitance, input resistance, resting membrane potential, AP amplitude, and the amplitude and duration of the afterhyperpolarization were not considerable. Compared with the control group (2.9 ± 0.2 ms, n = 13), the AP duration was significantly decreased in the SG neurons of the mTBI group (2.3 ± 0.5 ms, n = 12) and sTBI group (2.3 ± 0.4 ms, n = 14), respectively ($p < 0.05$ for the control vs. the mTBI and $p<0.05$ for the control vs. the sTBI). Compared with the sham-operated group (2.4 ± 0.2 ms, n = 10), the measure of excitability was significantly increased in the ICG neurons of the m TBI (3.1 ± 0.2 ms, n = 12) and sTBI (3.2 ± 0.3 ms, n = 13) groups, respectively ($p < 0.05$ for the control vs. the mTBI, and $p < 0.05$ for the control vs. the sTBI).

Table 4. Electrical properties of the SG and ICG neurons in sham and TBI groups

Parameters	SG			ICG		
	Sham (n=13)	mTBI (n=12)	sTBI (n=14)	Sham (n=10)	mTBI (n=12)	sTBI (n=13)
Capacitance (pA/pF)	48.2 ± 5.7	51.2 ± 5.3	51.9 ± 6.2	52.3 ± 4.8	53.3 ± 4.6	53 ± 5.2
Diameter (μm)	29.8 ± 1.5	31.2 ± 1.2	29.5 ± 1.4	31.2 ± 1.5	31.5 ± 1.3	30.4 ± 0.7
R_i (mΩ)	671 ± 11	732 ± 11	714 ± 13	732 ± 12	727 ± 15	713 ± 10
RMP(mV)	-52.1 ± 2.3	-53.1 ± 3.2	-52.2 ± 2.1	-53.1 ± 2.3	-55.7 ± 1.8	-54.3 ± 2.2
Rheobase (pA)	63 ± 5.1	43.1 ± 5.3*	40.3 ± 4.8*	72 ± 6.3	81 ± 3.6*	87± 4.9*
Threshold (mV)	-31 ± 0.7	-37.1±1.1**	-38.3 ±1.5***	-31.7 ± 1	-23.7 ± 1.5**	-21.2 ± 2***
AP amplitude (mV)	99 ±4.1	101 ± 4.7	100 ± 3.4	101.4 ± 2.2	99.5 ± 3.1	97.2 ± 3.5
AP duration (ms) at 0 mV	2.9 ± 0.2	2.3 ± 0.5*	2.3 ± 0.4*	2.4 ± 0.2	3.1 ± 0.2*	3.2 ± 0.3*
AHP amplitude (mV)	17.7 ± 0.6	18.5 ± 0.5	19 ± 0.8	17.6 ± 0.8	18.7 ± 0.5	19 ± 0.8
AHP duration (ms)	274 ± 27.6	250 ± 24.7	266± 28.5	253.6 ± 21.7	278.5 ± 21.5	282.7 ± 25.6

(R_i, input resistance; RMP, resting membrane potential; AP, action potential; AHP, afterhyperpolarization)

∗P < 0.01, *** p < 0.001 compared to sham-operated group

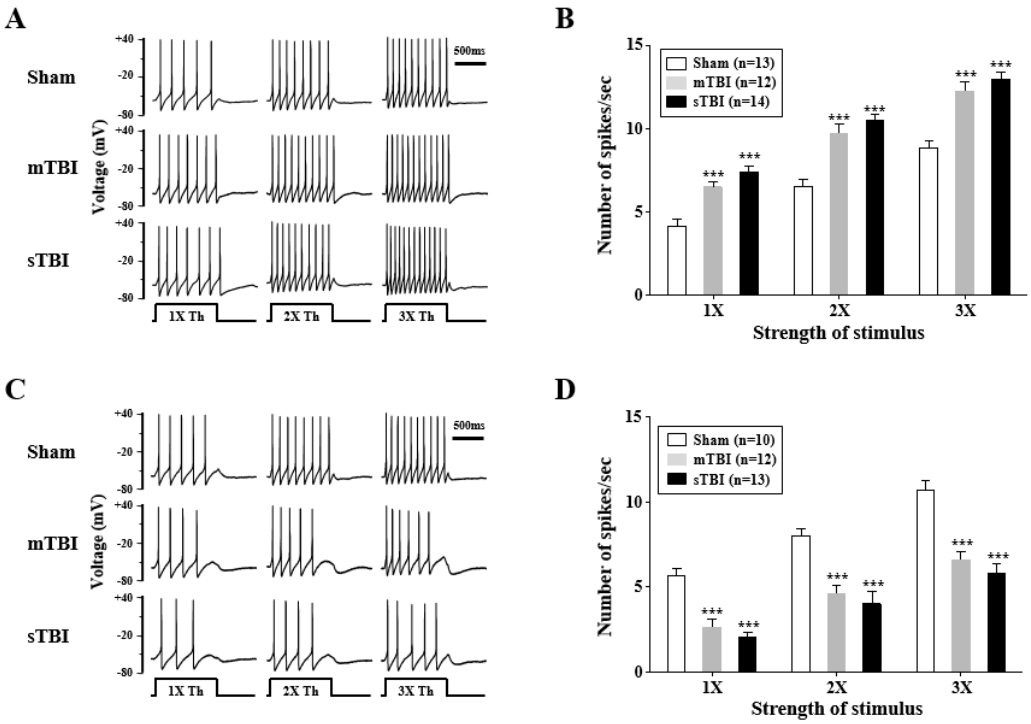

Figure 9. Changes in the excitability of SG and ICG neurons in TBI rats. **(A) and (C):** AP discharges in response to depolarizing current steps to 1, 2, and 3 times threshold (1X, 2X, and 3 X Th) for 1 s in the SG and ICG neurons, respectively from the sham, mTBI, and sTBI groups. Each neuron was depolarized from a resting membrane potential between -57 and -60 mV. **(B) and (D):** summary of the average number of spikes per second measured in A and C. Data are presented as the mean ± SEM. ***P < 0.001 compared with the sham group.

4.3. Decrease in the A-type K^+ currents in the SG neurons of the TBI groups

The voltage-dependent K^+ (K_V) channel is an important modulator of the activation threshold and spike discharge frequency in neurons (Xu et al., 2006). The major K_V currents in adult sympathetic neurons are known to be transient A-type K+ (K_A) and sustained delayed rectifier K^+ (K_{DR}) currents (Schofield et al., 1982). Therefore, we performed voltage-clamp recordings to test whether TBI affects K_A and K_{DR} currents in the SG neurons. The total outward K^+ (K_{Total}) and the K_{DR} currents were evoked using 1-s depolarizing test pulses between -50 mV and +20 mV from the holding potentials of -100 mV and -60 mV, respectively (Fig. 10A). K_A current traces were obtained by subtracting the K_{DR} current from the K_{Total} current (Phuket et al., 2009). As results, TBI significantly reduced the K_A current with little effect on the K_{DR} current. On average, the K_A current that was evoked using a test pulse of up to +20 mV was significantly decreased in the SG neurons of the mTBI group (63 ± 7 pA/pF, n = 12, $p < 0.05$) and sTBI group (47 ± 6 pA/pF, n = 14, $p<0.001$) compared with the control group (83 ± 6 pA/pF, n = 10) (Fig. 10B). The mean KDR current density was 132 ± 8 pA/pF (n = 10), 153 ± 11 pA/pF (n = 10), and 163 ± 16 pA/pF (n = 14) in the control, mTBI, and sTBI groups, respectively. The K_A current is lacking in adult ICG neurons, similar to neonatal ICG neurons (Xu et al., 1992). Similar to that in the SG neurons, the K_{DR} current in ICG neurons was not altered after TBI (data not shown).

In preliminary experiments using semi-quantitative RT-PCR, the SG

neurons from adult rats were found to express transcripts encoding different K_A channel α-subunits, including K_V4.1, K_V4.2, and K_V4.3 (Fig. 11A).

Consistent with the electrophysiological data, single-cell real-time PCR analysis revealed that the transcripts encoding the K_A channel α-subunits were significantly downregulated in the SG neurons of the TBI groups (Fig. 11B).

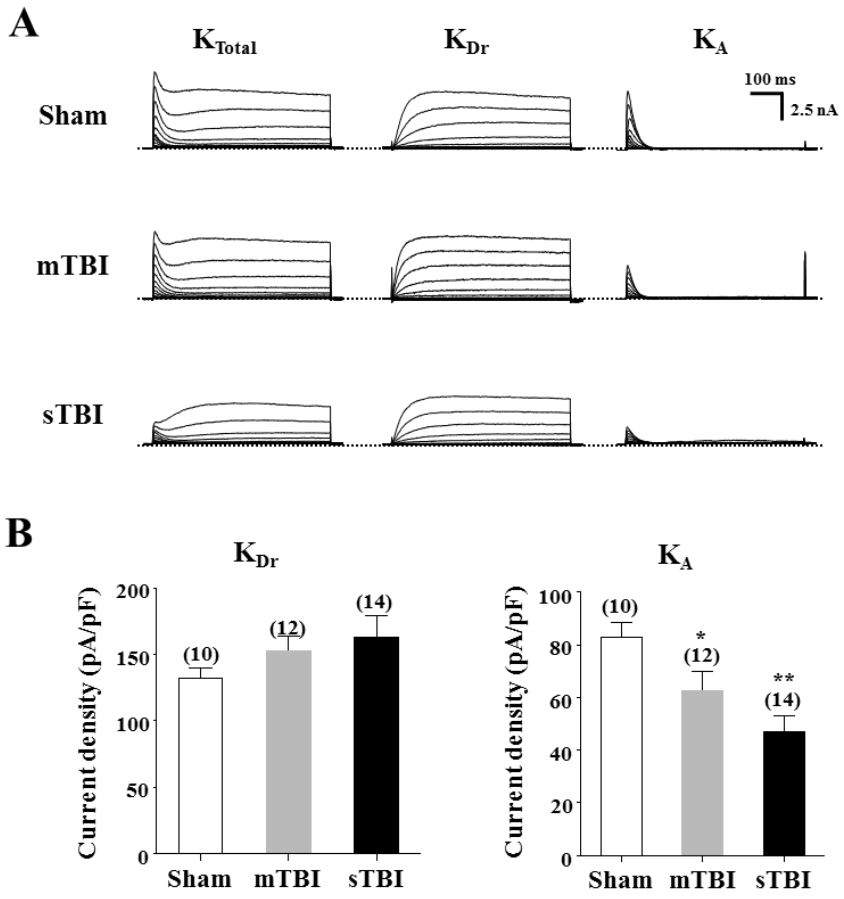

Figure 10. Effects of TBI on A-type and delayed rectifier K^+ currents in SG neurons. (A) Representative traces of total (K_{Total}), delayed rectifier (K_{DR}) and A-type (K_A) K^+ currents recorded in the SG neurons of the shame-operated, mTBI, and sTBI groups. The outward K_{Total} and the K_{DR} currents were evoked using 1-s depolarizing test pulses between -50 mV and +20 mV from the holding potentials of -100 mV and -60 mV, respectively. The K_A

current traces were obtained by subtracting the K_{DR} current from the K_{Total} current. **(B)** Summary of the K_{DR} and K_A current densities acquired with a test pulse to +20 mV in the SG neurons of the sham, mTBI, and sTBI groups. Data are presented as the means ± SEM. Number of neurons tested is indicated in parentheses. ***P < 0.001 compared with the sham-operated group.

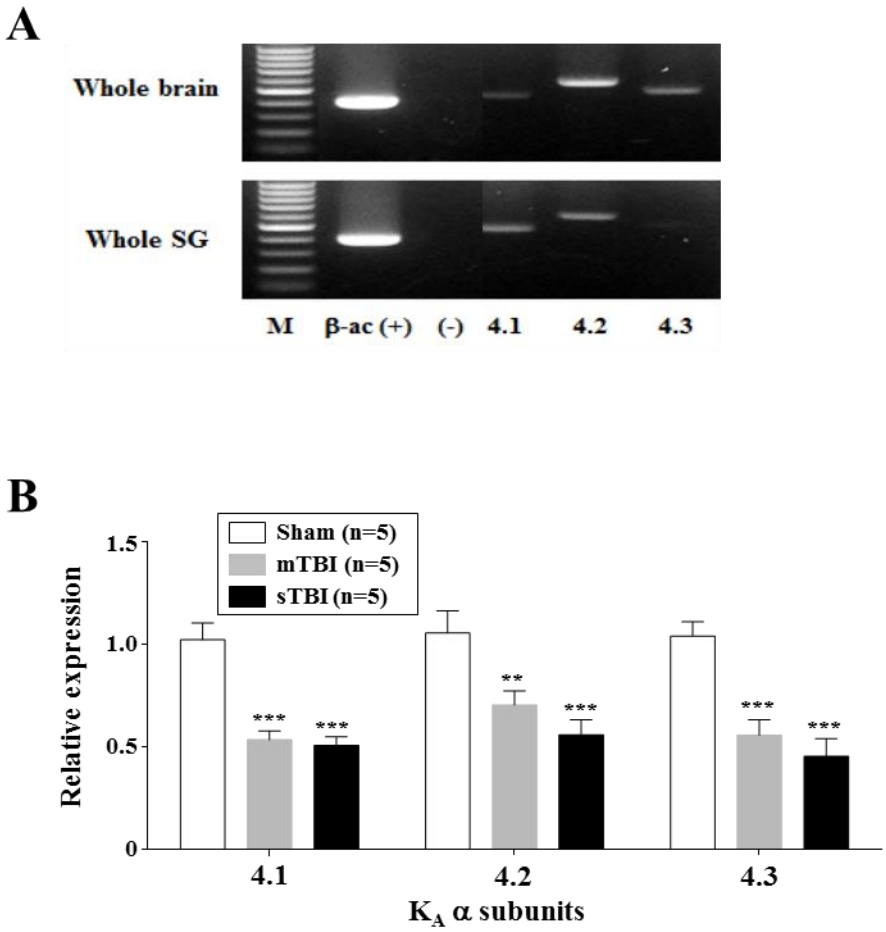

Figure 11. Downregulation of the K_A channel α-subunits expressed in the SG neurons from mTBI and sTBI groups. (A) Semi-quantitative RT-PCR shows that K_V4.1, K_V4.2, and K_V4.3 are expressed in rat SG neurons. Abbreviations in the figure are as follow: M, DNA size marker; β-ac, β-actin (an internal control). (-), No genomic DNA was detected in a parallel reaction

without reverse transcriptase. Whole-brain RNA was used as a positive control. **(B)** the relative expression levels of the transcripts encoding the K_A channel α-subunits, $K_V4.1$, $K_V4.2$, and $K_V4.3$ in the SG neurons of the mTBI, and sTBI groups. Data are presented as the means ± SEM. Number of neurons tested is indicated in parentheses. ***P < 0.001 compared with the sham group.

4.4. Opposite regulation of M-type K^+ current in the SG and ICG neurons of the TBI groups

Previous studies have shown that the slowly activating and deactivating M-type K+ (K_M) currents regulates the subthreshold electrical excitability and, thus, the spike discharge frequency (i.e., discharge pattern) in the sympathetic and parasympathetic postganglionic neurons (Brown et al., 1982; Cuevas et al. 1997; Xi-Moy et al., 1995). Consistent with these studies, XE-991 (3 μM), a selective K_M channel blocker, increased the spike discharge frequency in both SG and ICG neurons (Fig. 12A). To examine whether TBI alters the K_M current in the cardiac efferent neurons, the deactivation of K_M current was evoked using a test pulse to -60 mV for 500 ms from a holding potential of -30 mV (Fig. 12B). The K_M current was significantly decreased in the SG neurons of the TBI group (Fig. 12B). On average, the K_M current density in the SG neurons of the control, mTBI, and sTBI groups were 3 ± 0.3 pA/pF (n = 6), 1.9 ± 0.2 pA/pF (n = 7), and 1.8 ± 0.3pA/pF (n = 6), respectively (Fig. 12C). Conversely, the K_M current was significantly increased in the ICG neurons after TBI (Fig. 12B). On average, the K_M current density in the ICG neurons of the control, mTBI, and sTBI groups was 1.9 ± 0.3 pA/pF (n = 7), 3.2 ± 0.3 pA/pF (n = 6), and 3.5 ± 0.3pA/pF (n = 6), respectively (Fig. 12C). It is well known that the KCNQ2 and KCNQ3 channel subunits assemble to constitute the native K_M currents in the sympathetic neurons (Shapiro et al., 2000). Thus, we examined whether TBI regulates the expression of the transcripts encoding the KCNQ2 and KCNQ3 subunits

in the SG and ICG neurons. Single-cell real-time PCR analysis revealed that the transcript encoding KCNQ2 was approximately 2-fold down-regulated and up-regulated in the SG and ICG neurons of the TBI groups, respectively, compared with the control group (Fig. 12D). TBI did not alter the expression of the transcript encoding KCNQ3 in the SG and ICG neurons.

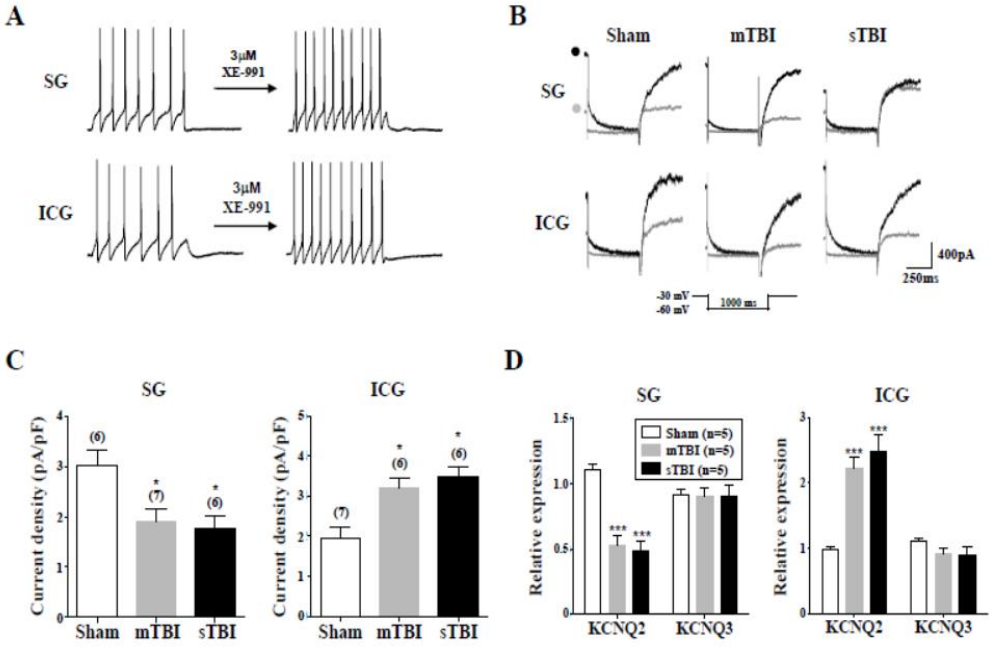

Figure 12. Opposite regulation of M-type K^+ current in the SG and ICG neurons of the TBI groups. (A) Effects of XE-991, a selective M-type K^+ (K_M) channel blocker on the AP discharge in SG and ICG neurons. (**B)** Representative K_M current traces recorded in the SG and ICG neurons of the sham, mTBI, and sTBI groups. The deactivation of K_M current was evoked using a test pulse to -60 mV for 500 ms from a holding potential of -30 mV in the absence (●) or presence (●) of XE-991(3 μM). **(C)** summary of the K_M current densities in the SG and ICG neurons of the shame-operated, mTBI, and sTBI groups. **(D)** The relative expression levels of the transcripts encoding the K_M channel subunits, KCNQ2 and KCNQ3 in the SG and ICG

neurons of the sham, mTBI, and sTBI groups. Data are presented as the means ± SEM. *P < 0.05, ***P < 0.001 compared with the sham group.

4.5. Alterations in the cell excitability of cardiac efferent neurons from the TBI groups

I examined whether TBI alters the cell excitability of arterial baroreceptor (AB) neurons in TBI rats. As shown in Fig. 13A, Di-I was injected into a part of the adventitia of the aortic arch to identify the AB neurons in the nodose ganglia. The small number of Di-I labeled AB neurons were detected by fluorescent microscopy (Fig. 13B). The AB neurons are composed of myelinated A-fiber (A-type) and unmyelinated C-fiber (C-type) neurons (Kraushs, 1979). The A- and C-type AB neurons can be easily distinguished by the presence or absence of capsaicin-sensitive TRPV1, and the shape and discharge properties of AP (Reynolds et al., 2006; Schild et al., 2012). As shown in Figure 13C, capsaicin (1 μM) evoked inward currents in C-type but not A-type AB neurons. Compared with A-type AB neurons, C-type AB neurons exhibit an AP with a definite inflection or “hump” during the repolarization phase which extends the AP duration of the action potential (Fig. 13C). In response to a strong depolarizing current (3 times threshold) injection for 1 sec, A-type AB neurons showed a regular and sustained AP discharge, while C-type AB neurons displayed a sparse and irregular discharge pattern (Fig. 13C).

Compared with sham group, the excitability of A-type AB neurons in mTBI and sTBI groups was significantly decreased and displayed only one or two action potentials in response to incremental depolarizing current stimulation (Fig. 14A) ($p < 0.001$ for sham vs. mTBI and $p < 0.001$ for sham vs. sTBI).

On average, the A-type AB neurons of sham group (n = 5) discharged at 7.4 ± 0.67, 12 ± 0.7, and 15.2 ± 1.012 spikes/sec, in response to 1X, 2X, and 3X threshold current stimulation, respectively. The A-type AB neurons of mTBI group (n = 7) discharged at 1.142 ± 0.17, 1.43 ± 0.21, and 2.3 ± 0.57 spikes/sec, and those of sTBI group (n = 6) discharged at 1.2 ± 0.1, 1.5 ± 0.3, and 1.8 ± 0.3 spikes/sec, in response to 1X, 2X, and 3X threshold current stimulation, respectively (Fig. 14B). The excitability of the C-type AB neurons was also significantly suppressed in mTBI and sTBI rats when they were stimulated with 2X and 3X threshold depolarizing currents (Fig. 15A) ($p < 0.001$ for sham vs. mTBI and $p < 0.001$ for sham vs. sTBI). On average, the C-type AB neurons of sham group (n = 6) discharged at 1.5 ± 0.37, 2.5 ± 0.4, and 3.7 ± 0.5 spikes/sec in response to 1X, 2X, and 3X threshold current stimulation, respectively. The C-type AB neurons of mTBI group (n = 8) discharged at 1.0, 1.5 ± 0.1 and 1.7 ± 0.35 spikes/sec, and those of sTBI group (n = 7) discharged at 1.0, 1.2 ± 0.2, and 1.4 ± 0.3 spikes/sec in response to 1X, 2X and 3X threshold current stimulation, respectively (Fig. 15B).

The passive and active properties of A- and C-type AB neurons in sham-control and TBI groups are summarized in Table 5 and Table 6. The altered excitability of AB neurons in TBI groups was also assessed by measuring the threshold potential and current threshold (rheobase) for triggering action potentials (Fig. 16). In this regard, the A-type AB neurons were stimulated with an incremental depolarizing current injection for 5 ms until single action potentials were generated (Fig.16A). Compared with sham group, the two

measures of excitability were significantly increased in the A-type AB neurons of TBI groups ($p < 0.001$ for sham vs. mTBI and $p < 0.001$ for sham vs. sTBI). On average, the threshold potentials were -31 ± 0.7 mV, -21 ± 1.1 mV, and -20.8 ± 1.5 mV in sham (n = 5), mTBI (n = 7), and sTBI (n = 7) groups, respectively (Fig. 16A & Table 5). The rheobases were 23 ± 4.1 pA, 143 ± 5.3 pA, and 180.3 ± 4.8 pA in sham, mTBI, and sTBI groups, respectively (Fig. 16A & Table 5). In C-type AB neurons, the TBI-induced change in excitability was also assessed by measuring the threshold potential and rheobase (Fig. 16B). The threshold potential was significantly increased in the C-type AB neurons of mTBI (-20.13 ± 1.0 mV, n = 7 $p < 0.001$) and sTBI (-18.1 ± 1.0 mV, n = 7, $p < 0.001$) groups compared with those of sham group (-31 ± 0.7 mV, n=5) (Fig. 16B & Table 6). In accordance with the changes in the threshold potential, the rheobase was also significantly increased in the C-type AB neurons of mTBI (251.5 ± 5.3 pA, $p < 0.001$) and sTBI (280.3 ± 4.8 pA, $p < 0.001$) groups compared with those of sham group (163 ± 5.1 pA) (Fig. 16B & Table 6). In addition to the threshold potential and rheobase, the durations of action potential and afterhyperpolarization (AHP) were also altered in the A- and C-type AB neurons of TBI groups (Tables 5 & 6).

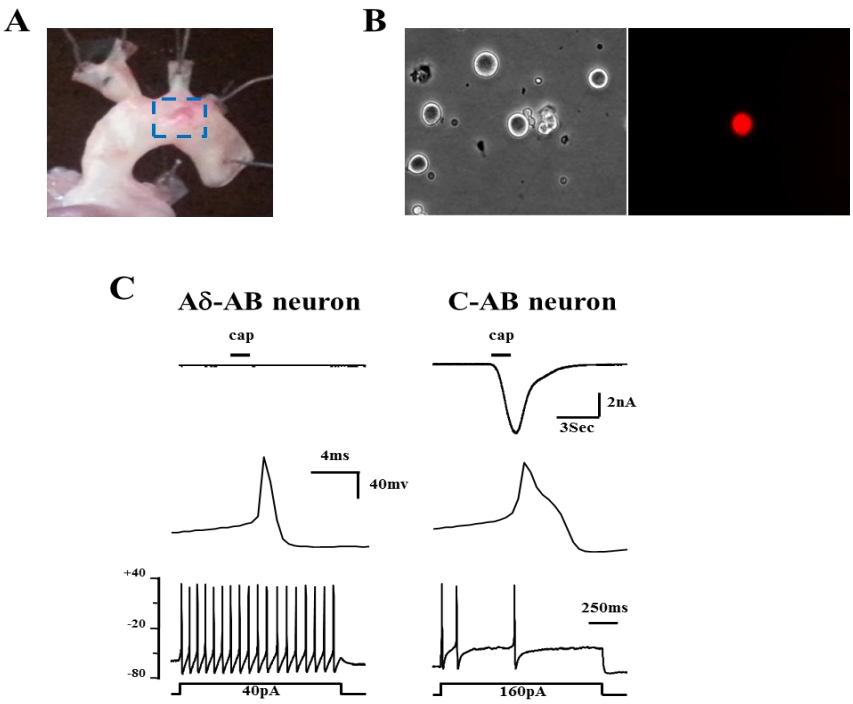

Figure 13. Identification of the A-type and C-type AB neurons in nodose ganglia. (A) DiI injection sites (the blue dotted box) on the aortic arch for retrograde labeling of the AB neurons. **(B)** Representative photomicrographs showing enzymatically dissociated nodose neurons (Left: a phase-contrast microscopic view) and an AB neuron retrogradely labeled with Di-I (Right: a fluorescent microscopic view at 200x). **(C)** Electrophysiological characterization of the Di-I labeled A-type and C-type AB neurons. Top: the responses to 1 μM capsaicin (cap). Middle: discharge of single action potentials in response to brief depolarizing current injection of threshold. Bottom: discharge of action potentials in response to strong depolarizing current (3 times threshold) injection for 1 second.

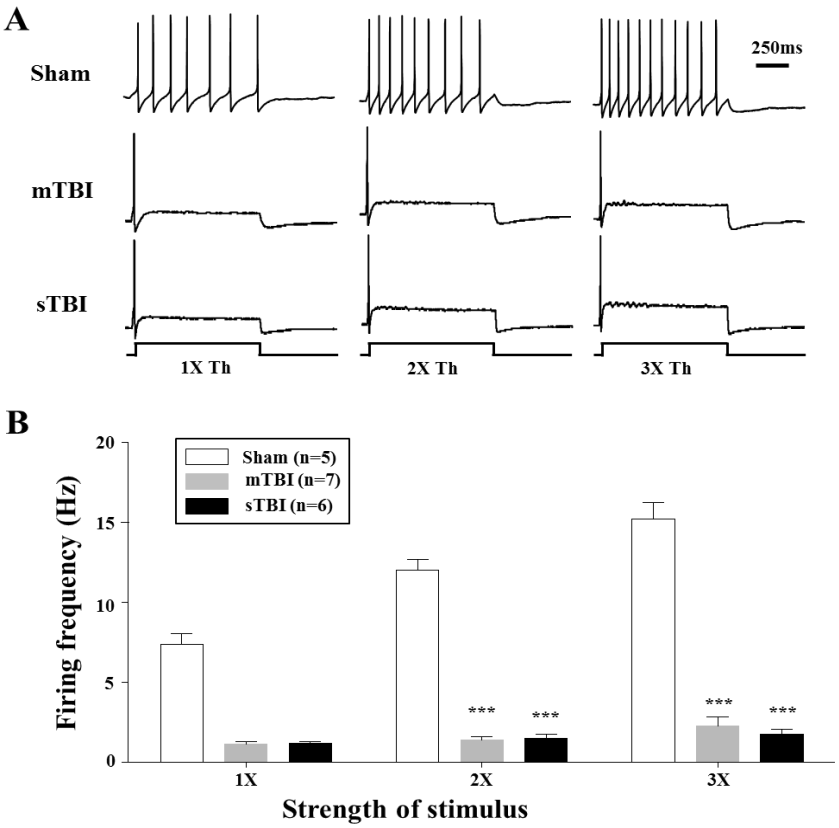

Figure 14. Changes in excitability of the A-type AB neurons in TBI groups. (A) Discharges of action potentials in response to depolarizing current steps to 1, 2, and 3 times-threshold (1X, 2X, and 3X Th) for 1 sec in the A-type and C-type AB neurons, respectively from sham, mTBI, and sTBI groups. The magnitude of 1X-Th stimulus (in pA) was shown on the AP traces. Spike firing was significantly reduced in TBI groups. Each neuron was depolarized from a resting membrane potential between -57 and -61 mV.

(B) Summary of mean number of spikes per second measured in A. Data are presented as the mean ± SEM. Number of neurons tested is indicated in parentheses. * $p < 0.05$, ** $p < 0.01$, *** $p < 0.001$ compared with sham group.

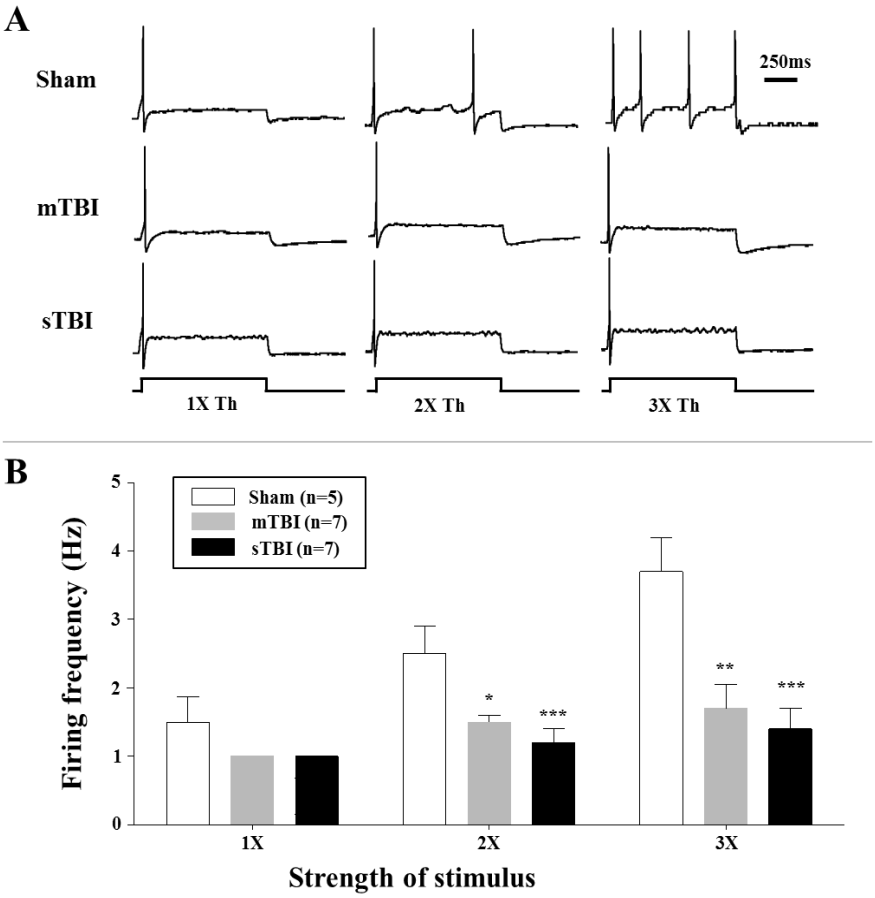

Figure 15. Changes in excitability of the C-type AB neurons in TBI groups. (A) Discharges of action potentials in response to depolarizing current steps to 1, 2, and 3 times-threshold (1X, 2X, and 3X Th) for 1 sec in C-type AB neurons, respectively from sham-contol, mTBI, and sTBI groups. The magnitude of 1X Th stimulus (in pA) was shown on the AP traces. Spike firing was significantly reduced in TBI groups. Each neuron was depolarized

from a resting membrane potential between -57 and -61 mV. **(B)** Summary of mean number of spikes per second measured in A. Data are presented as the mean ± SEM. Number of neurons tested is indicated in parentheses. * $p < 0.05$, ** $p < 0.01$, *** $p < 0.001$ compared with sham group.

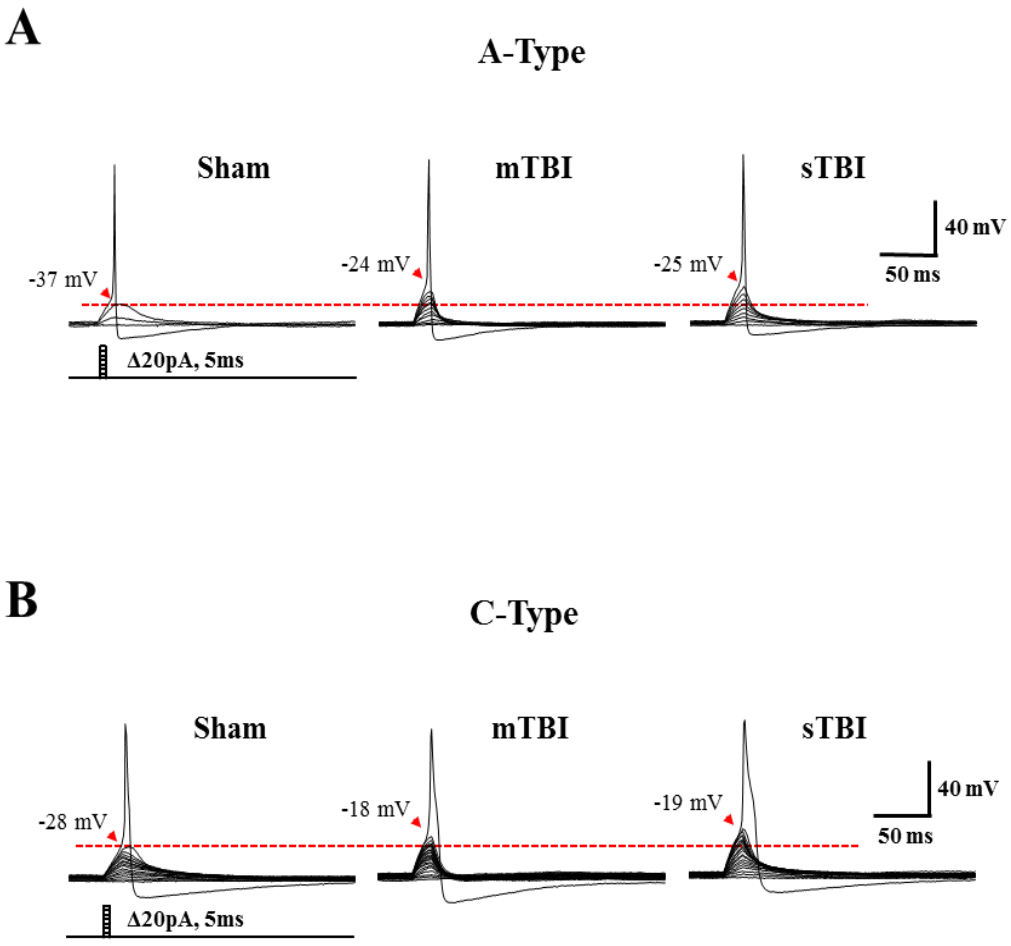

Figure 16. Increased threshold potential and rheobase in the A-type and C-type AB neurons of TBI groups. (A) & (B): Determination of threshold potential and rheobase in the A-type and C-type AB neurons, from sham, mTBI, and sTBI groups. The AB neurons were stimulated with incremental (△20pA) depolarizing current injection for 5ms until single action potentials were generated. The arrowheads indicate the threshold

potentials for the discharge of single action potentials. Each neuron was depolarized from a resting membrane potential between -58 and -63 mV.

Table 5. Electrophysiological characteristics of the Aδ-type AB neurons in TBI rats

Parameters	Sham (n=5)	mTBI (n=7)	sTBI (n=6)
Capacitance (pA/pF)	37.2 ± 3.7	38.2 ± 5.3	37.9 ± 4.2
Diameter (μm)	29.8 ± 1.5	31.2 ± 1.2	29.5 ± 1.4
R_i (mΩ)	871 ± 11	732 ± 11***	614 ± 13***
RMP(mV)	-52.1 ± 2.3	-53.1 ± 3.2	-52.2 ± 2.1
Rheobase (pA)	23 ± 4.1	143.1 ± 5.3***	180.3 ± 4.8***
Threshold (mV)	-31 ± 0.7	-21±1.1**	-20.8±1.5**
AP amplitude (mV)	108 ±4.1	101 ± 4.7	100 ± 3.4
AP duration (ms) at 0 mV	1.1 ± 0.2	2.1 ± 0.5*	2.3 ± 0.4*
AHP amplitude (mV)	15.7 ± 0.6	16.5 ± 0.5	17 ± 0.8
AHP duration (ms)	84 ± 17.6	150 ± 14.7*	166± 18.5*

(R_i , input resistance; RMP, resting membrane potential; AP, action potential; AHP, afterhyperpolarization)

(∗P < 0.01, *** p < 0.001 compared to control groups)

Table 6. Electrophysiological characteristics of the C-type AB neurons in TBI rats

Parameters	Sham (n=5)	mTBI (n=7)	sTBI (n=7)
Capacitance (pA/pF)	38.2 ± 2.7	41.2 ±.3.1	39.9 ± 3.2
Diameter (μm)	27.1 ± 1.5	30.2 ± 1.2	29.1 ± 1.0
R_i (mΩ)	371 ± 10	232 ± 8	213 ± 9
RMP(mV)	-52.1 ± 2.3	-53.1 ± 3.2	-53.1 ± 2.0
Rheobase (pA)	163 ± 5.1	251.5 ± 5.3***	280.3 ± 4.8***
Threshold (mV)	-31 ± 0.7	-20.1±1.0***	-18.1±1.0***
AP amplitude (mV)	99 ±4.1	101 ± 4.7	100 ± 3.4
AP duration (ms) at 0 mV	2.9 ± 0.2	3.8 ± 0.5*	4.3 ± 0.3*
AHP amplitude (mV)	17.7 ± 0.6	18.5 ± 0.5	19 ± 0.8
AHP duration (ms)	137 ± 7.6	180 ± 5.1*	186± 8.5*

(R_i, input resistance; RMP, resting membrane potential; AP, action potential; AHP, afterhyperpolarization)

(∗P < 0.01, *** p < 0.001 compared to control groups)

V. DISCUSSION

Many clinical studies have reported that the presence of CAD in patients with TBI increases morbidity and mortality, as well as the risk of progression to brain death. Despite the significance of probing the cellular mechanisms underlying the TBI-induced CAD, animal studies on this mechanism are lacking. To the best of my knowledge, the present study is the first to demonstrate that CAD develops during the post-insult sub-acute period in a rat model of TBI, as observed in human patients (Karen et al., 2005). Importantly, I demonstrated that (i) the TBI-induced CAD is associated with the opposing modulation of the excitability in the sympathetic and parasympathetic neurons innervating the heart, (ii) the opposite regulation of A- and/or M-type K+ channel currents underlie the altered excitability in these cardiac efferent neurons, and that (iii) TBI reduces the excitability of cardiac afferent neurons.

Brain injury is produced by a rigid impactor that delivers a focal mechanical insult to the intact dura in rat (Morganti-Kossmann et al., 2010). The levels of injury by moderate and severe TBI were determined via quantification of the cortical lesion volume and were comparable to the previous observation in rats (Yu et al. 2009). HRV and BRS were measured to assess whether CAD develops in TBI rats, as in TBI patients (Esterov and Greenwald, 2017; Hilz et al., 2010). These approaches have also been applied in a variety of animal models of myocardial infarction (Minisi et al., 2009), hypertension (da Silva et al., 2009), chronic heart failure (Zhang et al., 2015), cirrhosis (Lee et al.,

2016), diabetes (Gu et al., 2008), and sepsis (Radaelli et al., 2013). In the current study, CAD was observed, irrespective of TBI severity, which is consistent with clinical observations (Hilz et al., 2010). A recent clinical review has pointed out that even mild TBI can uncouple the autonomic control from the heart (Esterov and Greenwald, 2017). In the frequency domain analysis of HRV, the HF component is primarily associated with parasympathetic activity, whereas the LF component is largely under sympathetic control (Lombardi et al., 1996). Accordingly, the LF/HF ratio represents the balance between sympathetic and parasympathetic influences on the heart in rats (Kuwahara et al., 1994) and humans (Malliani et al., 1991; La Rovere et al., 2008). On the other hand, for assessing BRS, the reflexive bradycardia produced by a vasoconstrictor (i.e., PE) was measured in my experiments. Therefore, the acquired BRS may reflect the parasympathetic control at the sinoatrial node. Overall, the higher LF/HF ratio and lower BRS observed in TBI rats suggest an autonomic imbalance with sympathetic hyperactivity and parasympathetic hypoactivity.

The beat-to-beat reflexive control of the heart rate is mediated by the arterial baroreflex circuitry, which consists of peripheral afferent and efferent limbs, and central autonomic pathways in the brain stem. Thus, it could be presumed that TBI-induced CAD may arise from structural and functional alterations of the tracts or neurons at all levels of this reflex circuitry. In the current study, it was clarified whether TBI causes the functional plasticity of the peripheral efferent limb consisting of the sympathetic SG and parasympathetic ICG neurons. The axons of these cardiac efferent neurons

are in close physical proximity in the sinoatrial node for reciprocal modulation of the heart rate (Pardini et al., 1989). Conventionally, the autonomic efferent neurons have been considered as simple relays for conveying central autonomic outflows to target tissues. However, several lines of evidence have supported that the cardiac efferent ganglia themselves act as an integration center, where multiple extrinsic and intrinsic neural inputs are processed (Armour, 2007). Consistent with this notion, the functional plasticity at the level of the cardiac efferent neurons was found to be pivotal in the development of CAD in TBI rats. I showed that TBI increased the excitability of sympathetic SG neurons, while it decreased that of the parasympathetic ICG neurons. Indeed, the opposing regulation of excitability in these cardiac efferent neurons supports the autonomic imbalance observed in TBI rats.

Despite the pivotal role of SG neurons in the autonomic control of cardiac functions, little is known about the mechanisms controlling the excitability in these neurons. In general, voltage-gated K^+ (KV) channels are important determinants of the active AP properties in mammalian neurons (Ruby, 1988). Of these K_V channels, the K_A channel is known to be a determinant of the AP threshold and duration in the sympathetic superior cervical ganglion (SCG) neurons (Malin et al., 2001). The current study showed that spike discharge plasticity in the SG neurons of TBI rats is associated with a substantial reduction in the active membrane properties. Similar to the sympathetic superior cervical ganglion (SCG) neurons (Schofield et al., 1989; Gilbert et al., 1998), SG neurons were also found to display the K_V currents primarily

composed of transient K_A and sustained K_{DR} currents. Indeed, TBI selectively decreased the K_A, but not the K_{DR} currents, which may contribute to a reduced AP threshold and duration and the concomitant hyperexcitability of SG neurons. Several studies have demonstrated that Kv4 α subunits (KV4.1, KV4.2, and KV4.3) primarily underlie the K_A currents in the central neurons (Kim et al., 2005; Shibata et al. 2000) and SCG neurons (Malin and Nerbonne, 2000, 2001). In addition, the suppression of the K_V4.2 α subunit by a dominant negative mutant was found to enhance repetitive spike discharges in SCG neurons (Malin et al., 2001). I also found that the transcripts encoding all Kv4 α subunits are expressed in SG neurons, although the exact molecular correlates of the corresponding K_A currents remain to be defined. Importantly, the reduced K_A currents in the SG neurons of TBI rats may result from a downregulation of the Kv4 α subunit expression. Unlike the SG neurons, the K_A currents were not detected in the ICG neurons of adult rats, similar to neonatal ICG neurons (Xi-Moy et al., 1995). The K_M (KV7) channels are known to generate slowly activating and non-inactivating currents, in response to membrane depolarization, and determine the AP threshold and thus spike discharge frequency in the autonomic neurons (Brown et al., 1982; Wang and McKinnon, 1995; Arichi et al., 2019). Consistently, the application of XE-991, a selective K_M channel blocker, resulted in the hyperexcitability of rat SG and ICG neurons. A previous study reported that the K_M currents are not prominent in the guinea pig SG neurons (Gilbert et al., 1998). Thus, there appears to be species variation in the expression of the K_M currents. It is well known that the KCNQ2 and KCNQ3 channel subunits assemble to constitute

the native K_M currents in the sympathetic neurons (Shapiro et al., 2000). TBI causes the downregulation and upregulation of KCNQ2 mRNA transcripts and functional K_M currents, which may contribute to the hyperexcitability of the SG neurons and the hypoexcitability of the ICG neurons, respectively. The selective regulation of the KCNQ2 mRNA transcripts in the cardiac efferent neurons of TBI rats is consistent with the notion that K_M current expression in the peripheral nervous system is primarily determined by the regulation of KCNQ2 gene expression (Wang et al., 1998). It is unlikely that the altered excitability of cardiac efferent neurons is exclusively a result of the K_V (i.e., KA and KM) channel regulation. We previously demonstrated that the downregulation of voltage-gated Na+ (NaV) channels is associated with the hypoexcitability of the aortic baroreceptor neurons and the impairment of the arterial baroreflex in cirrhotic rats (Lee et al., 2016).

In the preliminary experiments, however, the NaV currents were not altered in the cardiac efferent neurons of TBI rats (J.W, Oh, and S.-W. Jeong, unpublished data). A previous study suggested that the selective inhibition of N-type Ca^{2+} currents decreases the excitability of SG and ICG neurons by reducing the AP threshold and duration (Tu et al., 2014). Thus, it might be worth examining whether TBI alters N-type Ca^{2+} channel expression and activity in the cardiac efferent neurons.

The TBI-induced CAD is speculated to arise from structural damage to the central autonomic nervous system, including the hypothalamus and the brain stem in human patients (Baguley et al., 2008). However, the current study suggests that the functional plasticity of the cardiac efferent neurons also

contributes to the development of CAD in TBI rats (Fig. 17). At present, it is unclear how the cortical insult remotely affects the peripheral autonomic neurons. Several studies have shown that TBI releases a variety of humoral factors, including catecholamine, stress hormones, inflammatory cytokines, and reactive oxygen species (ROS) into systemic circulation through the activation of multiple pathways (Lucas et al., 2006; Purkayastha, et al., 2019). Under certain pathological conditions such as chronic heart failure (Tu et al. 2010) and diabetes (Li et al., 2011), the reduced BRS and excitability of the aortic baroreceptor neurons appear to be associated with the angiotensin II-NADPH oxidase-ROS pathway. Interestingly, a previous study has shown that mild and moderate TBI activates the central angiotensin II-NADPH oxidase pathway for ROS production in the hypothalamic cardiovascular nuclei (Erdos et al., 2006). Accordingly, future studies should be directed at testing whether the aforementioned TBI-released factors, especially ROS, mediate the regulation of the K_V channel expression and the excitability of the cardiac efferent neurons.

A previous study has shown that that the functional plasticity of the aortic baroreceptor neurons is a potential mechanism underlying the impairment of the arterial baroreflex in cirrhotic rats (Lee et al., 2016). On the other hand, Gao et al. (2009) suggested that the downregulation of the Kv4.3 channel expression in sympathetic rostral ventrolateral medulla (RVLM) may contribute to sympathoexcitation in rats with chronic heart failure. Thus, besides the peripheral cardiac efferent neurons, the TBI-induced CAD could be attributed to any defects in the sensory pathways, including the peripheral

baroreceptor neurons and the second-order baroreceptor neurons in the nucleus tractus solitarius, and the motor pathways, including the sympathetic pressor center in the RVLM, the parasympathetic preganglionic neurons in the nucleus ambiguous and dorsal motor nucleus, and the spinal sympathetic preganglionic neurons in the arterial baroreflex circuitry. Indeed, TBI was found to affect the afferent limb of the baroreflex arc by dramatically decreasing the excitability of both A- and C-type AB neurons. Although the exact underlying mechanisms have yet to be resolved, each type of AB neurons is suggested to play a unique role in the processing of the mechanosensory information to the CNS to evoke the reflex responses (Schild and Kunze 2012). Thus, the hypoexcitability of A- and C-type AB neurons may contribute to the TBI-induced CAD (Fig. 17). In the future, studies of the second-order baroreceptor neurons of the nucleus tractus solitarius as well as in the central efferent neurons, including electrophysiology studies, are awaited.

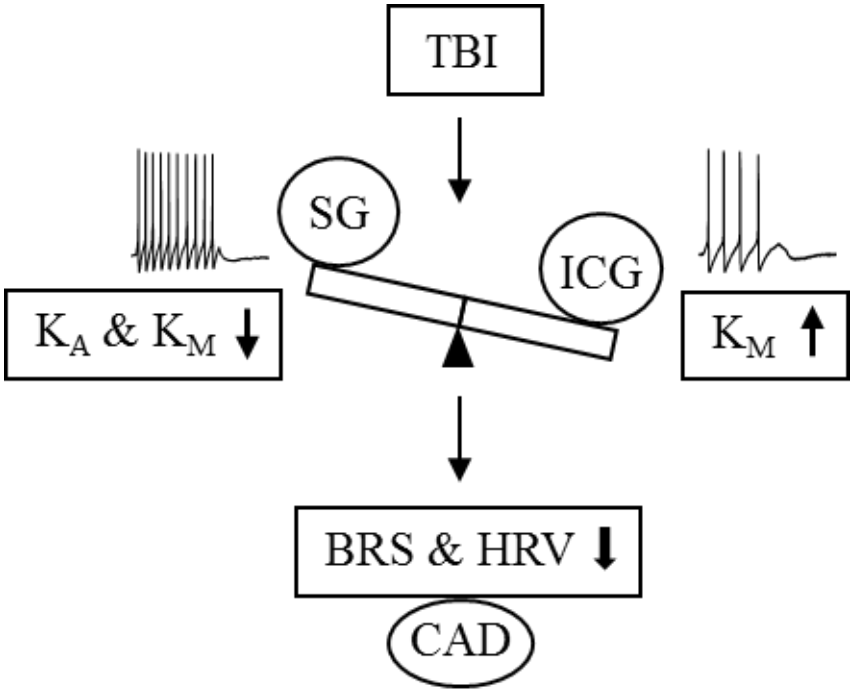

Figure 17. Schematic diagram showing the potential cellular mechanisms underlying TBI-induced CAD. TBI caused the development of CAD during post-insult sub-acute period irrespective of TBI severity. TBI increased the cell excitability in sympathetic SG neurons through downregulation of K_A and K_M currents, whereas decreased the cell excitability in parasympathetic ICG neurons through upregulation of K_M currents. The activity imbalance between these cardiac efferent neurons may contribute to the reduced HRV and BRS (CAD) in TBI rats.

VI. CONCLUSIONS

The CAD was developed during post-insult sub-acute period in a rat model of TBI. The key cellular mechanism underlying the TBI-induced CAD may be the functional plasticity of the peripheral cardiac efferent neurons, which is caused by the regulation of the K_A and/or K_M currents, and cardiac afferent neurons. Clinically, CAD is a commonly developed in different diseases including cirrhosis, portal hypertension, hear failure, and diabetes although pathogenesis is different. Thus, pre-clinical and clinical attention might be focused on probing common mediator(s) of the CAD regardless of origin.

VII. REFERENCES

Adams, D.J. , and A.A. Harper. 1995. *Electrophysiological Properties of Autonomic Ganglion Neurons.*

Adams, P. R., D. A. Brown, and A. Constanti. 1982. 'M-currents and other potassium currents in bullfrog sympathetic neurones', *J Physiol*, 330: 537-72.

Adams, P. R., and M. Galvan. 1986. 'Voltage-dependent currents of vertebrate neurons and their role in membrane excitability', *Adv Neurol*, 44: 137-70.

Adekoya, N., D. J. Thurman, D. D. White, and K. W. Webb. 2002. 'Surveillance for traumatic brain injury deaths--United States, 1989-1998', *MMWR Surveill Summ*, 51: 1-14.

Al Brashdi, Y. H., and M. S. Albayram. 2015. 'Reversible restricted-diffusion lesion representing transient intramyelinic cytotoxic edema in a patient with traumatic brain injury', *Neuroradiol J*, 28: 409-12.

Allen, T. G. J., and G. Burnstock. 1987. 'Intracellular Studies of the Electrophysiological Properties of Cultured Intracardiac Neurons of the Guinea-Pig', *Journal of Physiology-London*, 388: 349-66.

Andersson, B., G. Wallin, T. Hedner, A. C. Ahlberg, and O. K. Andersson. 1988. 'Acute effects of short-term fasting on blood pressure, circulating noradrenaline and efferent sympathetic nerve

activity', *Acta Med Scand*, 223: 485-90.

Arai, Y., J. P. Saul, P. Albrecht, L. H. Hartley, L. S. Lilly, R. J. Cohen, and W. S. Colucci. 1989. 'Modulation of Cardiac Autonomic Activity during and Immediately after Exercise', *American Journal of Physiology*, 256: H132-H41.

Behrens, M. I., C. Vergara, and R. Latorre. 1988. 'Calcium-activated potassium channels of large unitary conductance', *Brazilian Journal of Medical and Biological Research*, 21: 1101-17.

Behrens, S., and M. R. Franz. 2001. 'Circadian variation of arrhythmic events, electrophysiological properties, and the autonomic nervous system', *European Heart Journal*, 22: 2144-6.

Belavic, M., E. Jancic, P. Miskovic, A. Brozovic-Krijan, B. Bakota, and J. Zunic. 2015. 'Secondary stroke in patients with polytrauma and traumatic brain injury treated in an Intensive Care Unit, Karlovac General Hospital, Croatia', *Injury*, 46 Suppl 6: S31-5.

Belluzzi, O., and O. Sacchi. 1986. 'A Quantitative Description of the Sodium Current in the Rat Sympathetic Neuron', *Journal of Physiology-London*, 380: 275-91.

Belluzzi, O., O. Sacchi, and E. Wanke. 1985. 'A Fast Transient Outward Current in the Rat Sympathetic Neuron Studied under Voltage-Clamp Conditions', *Journal of Physiology-London*, 358: 91-108.

Bonds, B. W., S. Yang, P. F. Hu, K. Kalpakis, L. G. Stansbury, T. M. Scalea, and D. M. Stein. 2015. 'Predicting secondary insults after severe traumatic brain injury', *J Trauma Acute Care Surg*,

79: 85-90; discussion 90.

Brown, G. B. 1988. 'Batrachotoxin: a window on the allosteric nature of the voltage-sensitive sodium channel', *Int Rev Neurobiol*, 29: 77-116.

Caffrey, J. M., D. L. Eng, J. A. Black, S. G. Waxman, and J. D. Kocsis. 1992. 'Three types of sodium channels in adult rat dorsal root ganglion neurons', *Brain Res*, 592: 283-97.

Cai, G., K. Guo, D. Zhang, and S. Qin. 2020. 'The efficacy of baroreflex activation therapy for heart failure: A meta-analysis of randomized controlled trials', *Medicine (Baltimore)*, 99: e22951.

Canessa, C. M., J. D. Horisberger, and B. C. Rossier. 1993. 'Epithelial Sodium-Channel Related to Proteins Involved in Neurodegeneration', *Nature*, 361: 467-70.

Catterall, W. A., and A. P. Few. 2008. 'Calcium channel regulation and presynaptic plasticity', *Neuron*, 59: 882-901.

Catterall, W. A., A. L. Goldin, and S. G. Waxman. 2005. 'International Union of Pharmacology. XLVII. Nomenclature and structure-function relationships of voltage-gated sodium channels', *Pharmacol Rev*, 57: 397-409.

Chalfie, M., and E. Wolinsky. 1990. 'The identification and suppression of inherited neurodegeneration in Caenorhabditis elegans', *Nature*, 345: 410-6.

Chan, J. Y., S. M. Yang, and S. H. Chan. 1998. 'Mediation by N-methyl-D-aspartate and non-N-methyl-D-aspartate receptors in the

expression of Fos protein at the nucleus tractus solitarii in response to baroreceptor activation in the rat', *Neuroscience*, 83: 93-105.

Chen, J., S. R. Ikeda, W. Lang, C. M. Isales, and X. Wei. 1997. 'Molecular cloning of a putative tetrodotoxin-resistant sodium channel from dog nodose ganglion neurons', *Gene*, 202: 7-14.

Ciriello, J., C. G. Schultz, and S. Roder. 1994. 'Collateral axonal projections from ventrolateral medullary non-catecholaminergic neurons to central nucleus of the amygdala', *Brain Res*, 663: 346-51.

Clifton G. L., C. S. Robertson, K. Kyper, A. A. Taylor, R. D. Dhekne, and R. G. Grossman. 1983. ‘Cardiovascular response to severe head injury’, *J Neurosurg* 59: 447-454

Connor, J. A., and C. F. Stevens. 1971. 'Voltage clamp studies of a transient outward membrane current in gastropod neural somata', *J Physiol*, 213: 21-30.

Coronado, V. G., L. Xu, S. V. Basavaraju, L. C. McGuire, M. M. Wald, M. D. Faul, B. R. Guzman, J. D. Hemphill, Control Centers for Disease, and Prevention. 2011. 'Surveillance for traumatic brain injury-related deaths--United States, 1997-2007', *MMWR Surveill Summ*, 60: 1-32.

Cuevas, J. 2014. 'Molecular mechanisms of dysautonomia during heart failure. Focus on "Heart failure-induced changes of voltage-gated Ca2+ channels and cell excitability in rat cardiac

postganglionic neurons"', *American Journal of Physiology-Cell Physiology*, 306: C121-C22.

Cuevas, J., A. A. Harper, C. Trequattrini, and D. J. Adams. 1997. 'Passive and active membrane properties of isolated rat intracardiac neurons. Regulation by H- and M-currents', *Journal of Neurophysiology*, 78: 1890-902.

Cummins, T. R., P. L. Sheets, and S. G. Waxman. 2007. 'The roles of sodium channels in nociception: Implications for mechanisms of pain', *Pain*, 131: 243-57.

Czachurski, J., K. J. Lackner, D. Ockert, and H. Seller. 1982. 'Localization of neurones with baroreceptor input in the medial solitary nucleus by means of intracellular application of horseradish peroxidase in the cat', *Neurosci Lett*, 28: 133-7.

Daut, J. 1973. 'Modulation of the excitatory synaptic response by fast transient K+ current in snail neurones', *Nat New Biol*, 246: 193-6.

Dennis, M. J., A. J. Harris, and S. W. Kuffler. 1971. 'Synaptic transmission and its duplication by focally applied acetylcholine in parasympathetic neurons in the heart of the frog', *Proc R Soc Lond B Biol Sci*, 177: 509-39.

DeWitt, D. S., D. S. Prough, C. L. Taylor, and J. M. Whitley. 1992. 'Reduced cerebral blood flow, oxygen delivery, and electroencephalographic activity after traumatic brain injury and mild hemorrhage in cats', *J Neurosurg*, 76: 812-21.

Doan, T. N., and D. L. Kunze. 1999. 'Contribution of the hyperpolarization-activated current to the resting membrane potential of rat nodose sensory neurons', *J Physiol*, 514 (Pt 1): 125-38.

Doan, T. N., K. Stephans, A. N. Ramirez, P. A. Glazebrook, M. C. Andresen, and D. L. Kunze. 2004. 'Differential distribution and function of hyperpolarization-activated channels in sensory neurons and mechanosensitive fibers', *Journal of Neuroscience*, 24: 3335-43.

Doyle, M. W., and M. C. Andresen. 2001. 'Reliability of monosynaptic sensory transmission in brain stem neurons in vitro', *J Neurophysiol*, 85: 2213-23.

Driscoll, M., and M. Chalfie. 1991. 'The Mec-4 Gene Is a Member of a Family of Caenorhabditis-Elegans Genes That Can Mutate to Induce Neuronal Degeneration', *Nature*, 349: 588-93.

Drummond, H. A., N. L. Jernigan, and S. C. Grifoni. 2008. 'Sensing tension: epithelial sodium channel/acid-sensing ion channel proteins in cardiovascular homeostasis', *Hypertension*, 51: 1265-71.

Drummond, H. A., M. J. Welsh, and F. M. Abboud. 2001. 'ENaC subunits are molecular components of the arterial baroreceptor complex', *Neuro-Cardiovascular Regulation: From Molecules to Man*, 940: 42-47.

Duggan, A., J. Garcia-Anoveros, and D. P. Corey. 2002. 'The PDZ

domain protein PICK1 and the sodium channel BNaC1 interact and localize at mechanosensory terminals of dorsal root ganglion neurons and dendrites of central neurons', *Journal of Biological Chemistry*, 277: 5203-08.

Dunlap, K., J. I. Luebke, and T. J. Turner. 1995. 'Exocytotic Ca2+ channels in mammalian central neurons', *Trends Neurosci*, 18: 89-98.

Franciosi, S., F. K. G. Perry, T. M. Roston, K. R. Armstrong, V. E. Claydon, and S. Sanatani. 2017. 'The role of the autonomic nervous system in arrhythmias and sudden cardiac death', *Auton Neurosci*, 205: 1-11.

Franklin, J. L., and A. L. Willard. 1993. 'Voltage-Dependent Sodium and Calcium Currents of Rat Myenteric Neurons in Cell-Culture', *Journal of Neurophysiology*, 69: 1264-75.

Freschi, J. E. 1983. 'Membrane Currents of Cultured Rat Sympathetic Neurons under Voltage Clamp', *Journal of Neurophysiology*, 50: 1460-78.

Galvan, M. 1982. 'A transient outward current in rat sympathetic neurones', *Neurosci Lett*, 31: 295-300.

Galvan, M., and C. Sedlmeir. 1984a. 'Outward currents in voltage-clamped rat sympathetic neurones', *J Physiol*, 356: 115-33.

Gilbert, R., J. S. Ryan, M. Horackova, F. M. Smith, and M. E. M. Kelly. 1998. 'Actions of substance P on membrane potential and ionic currents in guinea pig stellate ganglion neurons', *American*

Journal of Physiology-Cell Physiology, 274: C892-C903.

Goldberger, J. J., R. Arora, U. Buckley, and K.Shivkumar. 2019. 'Autonomic Nervous System Dysfunction: JACC Focus Seminar', *J Am Coll Cardiol.* 73:1189-1206.

Goldstein, B., D. Toweill, S. Lai, K. Sonnenthal, and B. Kimberly. 1998. 'Uncoupling of the autonomic and cardiovascular systems in acute brain injury', *American Journal of Physiology-Regulatory Integrative and Comparative Physiology*, 275: R1287-R92.

Gordon, F. J. 1995. 'Excitatory amino acid receptors in central cardiovascular regulation', *Clin Exp Hypertens*, 17: 81-90.

Gordon, R., J. V. Reid, A. Sjoerdsma, and S. Udenfriend. 1966. 'Increased synthesis of norepinephrine in the rat heart on electrical stimulation of the stellate ganglia', *Mol Pharmacol*, 2: 610-3.

Hardwick, J. C., G. M. Mawe, and R. L. Parsons. 1995. 'Evidence for afferent fiber innervation of parasympathetic neurons of the guinea-pig cardiac ganglion', *J Auton Nerv Syst*, 53: 166-74.

Hassankhani, A., M. E. Steinhelper, M. H. Soonpaa, E. B. Katz, D. A. Taylor, A. Andraderozental, S. M. Factor, J. J. Steinberg, L. J. Field, and H. J. Federoff. 1995. 'Overexpression of Ngf within the Heart of Transgenic Mice Causes Hyperinnervation, Cardiac Enlargement, and Hyperplasia of Ectopic Cells', *Developmental Biology*, 169: 309-21.

Henden, P. L., S. Sondergaard, B. Rydenhag, B. Reinsfelt, S. E.

Ricksten, and A. Aring;neman. 2014. 'Can Baroreflex Sensitivity and Heart Rate Variability Predict Late Neurological Outcome in Patients With Traumatic Brain Injury?', *Journal of Neurosurgical Anesthesiology*, 26: 50-59.

Hendrickse, M. T., and D. R. Triger. 1992. 'Peripheral and Cardiovascular Autonomic Impairment in Chronic Liver-Disease - Prevalence and Relation to Hepatic-Function', *Journal of Hepatology*, 16: 177-83.

Herat, L. Y., M. P. Schlaich, and V. B. Matthews. 2019. 'Sympathetic stimulation with norepinephrine may come at a cost', *Neural Regen Res*, 14: 977-78.

Hille, B. 1992. 'Axons, ions, and dons', *Science*, 258: 144-5.

Ikeda, S. R., and G. G. Schofield. 1987. 'Tetrodotoxin-resistant sodium current of rat nodose neurones: monovalent cation selectivity and divalent cation block', *J Physiol*, 389: 255-70.

Ikeda, S. R., G. G. Schofield, and F. F. Weight. 1986. 'Na+ and Ca2+ currents of acutely isolated adult rat nodose ganglion cells', *J Neurophysiol*, 55: 527-39.

Jacobowitz, D. 1967. 'Histochemical studies of the relationship of chromaffin cells and adrenergic nerve fibers to the cardiac ganglia of several species', *J Pharmacol Exp Ther*, 158: 227-40.

Javorka, M., I. Zila, T. Balharek, and K. Javorka. 2003. 'On- and off-responses of heart rate to exercise - relations to heart rate variability', *Clinical Physiology and Functional Imaging*, 23: 1-8.

Jeong, S. W., and R. D. Wurster. 1997. 'Calcium channel currents in acutely dissociated intracardiac neurons from adult rats', *Journal of Neurophysiology*, 77: 1769-78.

Jeong, Y. H., J. Oh, and S. Cho. 2016. 'Clinical Outcome of Acute Epidural Hematoma in Korea: Preliminary Report of 285 Cases Registered in the Korean Trauma Data Bank System', *Korean J Neurotrauma*, 12: 47-54.

Jeske, I., S. F. Morrison, S. L. Cravo, and D. J. Reis. 1993. 'Identification of baroreceptor reflex interneurons in the caudal ventrolateral medulla', *American Journal of Physiology*, 264: R169-78.

Johannigman, J. A., D. Zonies, J. Dubose, T. C. Blakeman, D. Hanseman, and R. D. Branson. 2015. 'Reducing secondary insults in traumatic brain injury', *Mil Med*, 180: 50-5.

Katada, R., Y. Nishitani, O. Honmou, K. Mizuo, S. Okazaki, K. Tateda, S. Watanabe, and H. Matsumoto. 2012. 'Expression of aquaporin-4 augments cytotoxic brain edema after traumatic brain injury during acute ethanol exposure', *Am J Pathol*, 180: 17-23.

Katz, B. 1950. 'Action potentials from a sensory nerve ending', *J Physiol*, 111: 248-60.

Kaufman, M. P., B. R. Botterman, W. J. Gonyea, G. A. Iwamoto, and J. H. Mitchell. 1982. 'Cardiovascular Control during Static Exercise - Central and Reflex Neural Mechanisms', *Developments in Neuroscience*, 15: 97-107.

Kaufmann, D. K., G. Raczak, M. Szwoch, E. Wabich, M. Swiatczak, and L. Danilowicz-Szymanowicz. 2020. 'Baroreflex sensitivity but not microvolt T-wave alternans can predict major adverse cardiac events in ischemic heart failure', *Cardiol J*.

Keren, O., S. Yupatov, M. M. Radai, R. Elad-Yarum, D. Faraggi, S. Abboud, H. Ring, and Z. Groswasser. 2005. 'Heart rate variability (HRV) of patients with traumatic brain injury (TBI) during the post-insult sub-acute period', *Brain Injury*, 19: 605-611

Khalid, F., G. L. Yang, J. L. McGuire, M. J. Robson, B. Foreman, L. B. Ngwenya, and J. N. Lorenz. 2019. ‘Autonomic dysfunction following traumatic brain injury: translational insights’, *Neurosurg Focus* 47:E8.

King, M. L., S. W. Lichtman, G. Seliger, F. A. Ehert, and J. S. Steinberg. 1997. 'Heart-rate variability in chronic traumatic brain injury', *Brain Injury*, 11: 445-53.

Kobayashi, S. 1982. '[Classification of computerized tomography and prognosis of traumatic primary brain stem injury]', *Neurol Med Chir (Tokyo)*, 22: 838-48.

Konopka, L. M., L. A. Merriam, J. C. Hardwick, and R. L. Parsons. 1992. 'Aminergic and peptidergic elements and actions in a cardiac parasympathetic ganglion', *Can J Physiol Pharmacol*, 70 Suppl: S32-43.

Krishnamurthy, K., and D. T. Laskowitz. 2016. 'Cellular and Molecular

Mechanisms of Secondary Neuronal Injury following Traumatic Brain Injury.' in D. Laskowitz and G. Grant (eds.), *Translational Research in Traumatic Brain Injury* (Boca Raton (FL)).

Kumagai, H., N. Oshima, T. Matsuura, K. Iigaya, M. Imai, H. Onimaru, K. Sakata, M. Osaka, T. Onami, C. Takimoto, T. Kamayachi, H. Itoh, and T. Saruta. 2012. 'Importance of rostral ventrolateral medulla neurons in determining efferent sympathetic nerve activity and blood pressure', *Hypertens Res*, 35: 132-41.

Kwong, K., M. J. Carr, A. Gibbard, T. J. Savage, K. Singh, J. Jing, S. Meeker, and B. J. Undem. 2008. 'Voltage-gated sodium channels in nociceptive versus non-nociceptive nodose vagal sensory neurons innervating guinea pig lungs', *J Physiol*, 586: 1321-36.

Lacassagne, O., and J. P. Kessler. 2000. 'Cellular and subcellular distribution of the amino-3-hydroxy-5-methyl-4-isoxazole propionate receptor subunit GluR2 in the rat dorsal vagal complex', *Neuroscience*, 99: 557-63.

Lai, C. Q., H. Ibrahim, A. I. Abd Hamid, and J. M. Abdullah. 2020. 'Classification of Non-Severe Traumatic Brain Injury from Resting-State EEG Signal Using LSTM Network with ECOC-SVM', *Sensors (Basel)*, 20.

Lane, M. A., A. Sastre, and M. M. Salpeter. 1976. 'Innervation of heart cells in culture by an endogenous source of cholinergic neurons', *Proc Natl Acad Sci U S A*, 73: 4506-10.

Lanfranchi, P. A., and V. K. Somers. 2002. 'Arterial baroreflex function and cardiovascular variability: interactions and implications', *American Journal of Physiology-Regulatory Integrative and Comparative Physiology*, 283: R815-R26.

Langlois, J. A., S. R. Kegler, J. A. Butler, K. E. Gotsch, R. L. Johnson, A. A. Reichard, K. W. Webb, V. G. Coronado, A. W. Selassie, and D. J. Thurman. 2003. 'Traumatic brain injury-related hospital discharges. Results from a 14-state surveillance system, 1997', *MMWR Surveill Summ*, 52: 1-20.

Li, B. Y., G. F. Qiao, B. Feng, R. B. Zhao, Y. J. Lu, and J. H. Schild. 2008. 'Electrophysiological and neuroanatomical evidence of sexual dimorphism in aortic baroreceptor and vagal afferents in rat', *Am J Physiol Regul Integr Comp Physiol*, 295: R1301-10.

Li, B. Y., and J. H. Schild. 2007. 'Electrophysiological and pharmacological validation of vagal afferent fiber type of neurons enzymatically isolated from rat nodose ganglia', *J Neurosci Methods*, 164: 75-85.

Li, Y., Y. Feng, L. Liu, X. Li, X. Y. Li, X. Sun, K. X. Li, R. R. Zha, H. D. Wang, M. D. Zhang, X. X. Fan, D. Wu, Y. Fan, H. C. Zhang, G. F. Qiao, and B. Y. Li. 2020. 'The baroreflex afferent pathway plays a critical role in H2S-mediated autonomic control of blood pressure regulation under physiological and hypertensive conditions', *Acta Pharmacologica Sinica*.

Liu, M., and J. N. Wood. 2011. 'The roles of sodium channels in

nociception: implications for mechanisms of neuropathic pain', *Pain Med*, 12 Suppl 3: S93-9.

Llewellyn-Smith, I. J., P. Pilowsky, J. B. Minson, and J. Chalmers. 1995. 'Synapses on axons of sympathetic preganglionic neurons in rat and rabbit thoracic spinal cord', *J Comp Neurol*, 354: 193-208.

Lu, H., and X. Lei. 2014. 'The apparent diffusion coefficient does not reflect cytotoxic edema on the uninjured side after traumatic brain injury', *Neural Regen Res*, 9: 973-7.

Ludwig, A., X. Zong, J. Stieber, R. Hullin, F. Hofmann, and M. Biel. 1999. 'Two pacemaker channels from human heart with profoundly different activation kinetics', *EMBO J*, 18: 2323-9.

Ma, X., A. Aravind, B. J. Pfister, N. Chandra, and J. Haorah. 2019. 'Animal Models of Traumatic Brain Injury and Assessment of Injury Severity', *Mol Neurobiol*, 56: 5332-5345

Maas, X., A. Aravind, B. J. Pfister, N. Chandra, and J. Haorah. 2017. 'Traumatic brain injury: integrated approaches to improve prevention, clinical care, and research'. *Lancet Neurol*, 17: 987-1048

Mangoni, M. E., B. Couette, L. Marger, E. Bourinet, J. Striessnig, and J. Nargeot. 2006. 'Voltage-dependent calcium channels and cardiac pacemaker activity: from ionic currents to genes', *Prog Biophys Mol Biol*, 90: 38-63.

Marquez, M. F., J. R. Gomez-Flores, J. A. Gonzalez-Hermosillo, T. J. Ruiz-Siller, and M. Cardenas. 2016. '[Role of the sympathetic

nervous system in vasovagal syncope and rationale for beta-blockers and norepinephrine transporter inhibitors]', *Medwave*, 16: e6824.

McCarthy, R. T., and P. E. TanPiengco. 1992. 'Multiple types of high-threshold calcium channels in rabbit sensory neurons: high-affinity block of neuronal L-type by nimodipine', *Journal of Neuroscience*, 12: 2225-34.

Mcdonald, F. J., and M. J. Welsh. 1995. 'Binding of the Proline-Rich Region of the Epithelial Na+ Channel to Sh3 Domains and Its Association with Specific Cellular Proteins', *Biochemical Journal*, 312: 491-97.

Meeley, M. P., M. D. Underwood, W. T. Talman, and D. J. Reis. 1989. 'Content and in vitro release of endogenous amino acids in the area of the nucleus of the solitary tract of the rat', *J Neurochem*, 53: 1807-17.

Mendelowitz, D., M. Yang, M. C. Andresen, and D. L. Kunze. 1992. 'Localization and retention in vitro of fluorescently labeled aortic baroreceptor terminals on neurons from the nucleus tractus solitarius', *Brain Res*, 581: 339-43.

Mitchell, J. H. 1985. 'Cardiovascular Control during Exercise - Central and Reflex Neural Mechanisms', *American Journal of Cardiology*, 55: D34-D41.

Miyoshi, M., H. Kondo, Y. Ishii, T. Shinohara, K. Yonezu, T. Harada, H. Sato, Y. Yano, S. Yoshimura, I. Abe, T. Shuto, H. Akioka, Y.

Teshima, T. Wada, K. Yufu, M. Nakagawa, H. Anai, S. Miyamoto, and N. Takahashi. 2020. 'Baroreflex Sensitivity in Patients With Atrial Fibrillation', *J Am Heart Assoc*: e018019.

Moravec, M., J. Moravec, and S. Forsgren. 1990. 'Catecholaminergic and peptidergic nerve components of intramural ganglia in the rat heart. An immunohistochemical study', *Cell Tissue Res*, 262: 315-27.

Morrison, S. F., and D. J. Reis. 1991. 'Responses of sympathetic preganglionic neurons to rostral ventrolateral medullary stimulation', *American Journal of Physiology*, 261: R1247-56.

Muroi, Y., F. Ru, M. Kollarik, B. J. Canning, S. A. Hughes, S. Walsh, M. Sigg, M. J. Carr, and B. J. Undem. 2011. 'Selective silencing of Na(V)1.7 decreases excitability and conduction in vagal sensory neurons', *J Physiol*, 589: 5663-76.

Nakagawa, A., K. Ohtani, K. Goda, D. Kudo, T. Arafune, T. Washio, and T. Tominaga. 2016. 'Mechanism of Traumatic Brain Injury at Distant Locations After Exposure to Blast Waves: Preliminary Results from Animal and Phantom Experiments', *Acta Neurochir Suppl*, 122: 3-7.

Page, P. L., N. Dandan, R. Cardinal, and R. Nadeau. 1995. '[Comparison of the infusion of acetylcholine into the artery of the sinoatrial node with the electric stimulation of cardiac parasympathetic nerves]', *Ann Chir*, 49: 719-27.

Parsons, R. L., D. S. Neel, T. W. McKeon, and R. E. Carraway. 1987.

'Organization of a vertebrate cardiac ganglion: a correlated biochemical and histochemical study', *Journal of Neuroscience*, 7: 837-46.

Patel, H. J., P. Venkatesan, J. Halfpenny, M. H. Yacoub, A. Fox, P. J. Barnes, and M. G. Belvisi. 1999. 'Modulation of acetylcholine release from parasympathetic nerves innervating guinea-pig and human trachea by endomorphin-1 and -2', *Eur J Pharmacol*, 374: 21-4.

Pearn, M.L., I. R. Niesman, J. Egawa, A. Sawada, A. Almenar-Queralt, S. B. Shah, J. L. Duckworth, B. P. Head. 2017. ‘Pathophysiology Associated with Traumatic Brain Injury: Current Treatments and Potential Novel Therapeutics’, *Cell Mol Neurobiol*. 37:571-585.

Perez-Alfayate, R., and K. Sallabanda-Diaz. 2019. 'Primary bilateral fronto-temporoparietal decompressive craniectomy-An alternative treatment for severe traumatic brain injury: Case report and technical note', *Clin Case Rep*, 7: 1031-39.

Persson, P. B., M. DiRienzo, P. Castiglioni, C. Cerutti, M. Pagani, N. Honzikova, S. Akselrod, and G. Parati. 2001. 'Time versus frequency domain techniques for assessing baroreflex sensitivity', *Journal of Hypertension*, 19: 1699-705.

Petry, D., C. Mirian de Godoy Marques, and J. L. Brum Marques. 2020. 'Baroreflex sensitivity with different lags and random forests for staging cardiovascular autonomic neuropathy in subjects with diabetes', *Comput Biol Med*, 127: 104098.

Pham, G. S., L. A. Wang, and K. W. Mathis. 2018. 'Pharmacological potentiation of the efferent vagus nerve attenuates blood pressure and renal injury in a murine model of systemic lupus erythematosus', *Am J Physiol Regul Integr Comp Physiol*, 315: R1261-R71.

Pilowsky, P., I. J. Llewellyn-Smith, J. Minson, and J. Chalmers. 1992. 'Sympathetic preganglionic neurons in rabbit spinal cord that project to the stellate or the superior cervical ganglion', *Brain Res*, 577: 181-8.

Plummer, M. R., D. E. Logothetis, and P. Hess. 1989. 'Elementary Properties and Pharmacological Sensitivities of Calcium Channels in Mammalian Peripheral Neurons', *Neuron*, 2: 1453-63.

Punchak, M., J. Abdelgadir, O. Obiga, M. Itait, J. N. Najjuma, M. M. Haglund, and D. Kitya. 2018. 'Mechanism of Pediatric Traumatic Brain Injury in Southwestern Uganda: A Prospective Cohort of 100 Patients', *World Neurosurg*, 114: e396-e402.

Rama Rao, K. V., S. Iring, D. Younger, M. Kuriakose, M. Skotak, E. Alay, R. K. Gupta, and N. Chandra. 2018. 'A Single Primary Blast-Induced Traumatic Brain Injury in a Rodent Model Causes Cell-Type Dependent Increase in Nicotinamide Adenine Dinucleotide Phosphate Oxidase Isoforms in Vulnerable Brain Regions', *J Neurotrauma*, 35: 2077-90.

Regan, L. J., D. W. Y. Sah, and B. P. Bean. 1991. 'Ca2+ Channels in Rat

Central and Peripheral Neurons - High-Threshold Current Resistant to Dihydropyridine Blockers and Omega-Conotoxin', *Neuron*, 6: 269-80.

Reynolds, P. J., W. Fan, and M. C. Andresen. 2006. 'Capsaicin-resistant arterial baroreceptors', *J Negat Results Biomed*, 5: 6.

Roskoski, R., Jr., R. I. McDonald, L. M. Roskoski, W. J. Marvin, and K. Hermsmeyer. 1977. 'Choline acetyltransferase activity in heart: evidence for neuronal and not myocardial origin', *American Journal of Physiology*, 233: H642-6.

Roy, M. L., and T. Narahashi. 1992. 'Differential properties of tetrodotoxin-sensitive and tetrodotoxin-resistant sodium channels in rat dorsal root ganglion neurons', *Journal of Neuroscience*, 12: 2104-11.

Santoro, B., and G. R. Tibbs. 1999. 'The HCN gene family: molecular basis of the hyperpolarization-activated pacemaker channels', *Ann N Y Acad Sci*, 868: 741-64.

Schaffar, N., J. Pio, and A. Jean. 1990. 'Selective retrograde labeling of primary vagal afferent cell-bodies after injection of [3H]D-aspartate into the rat nucleus tractus solitarii', *Neurosci Lett*, 114: 253-8.

Schild, J. H., and D. L. Kunze. 1997. 'Experimental and modeling study of Na+ current heterogeneity in rat nodose neurons and its impact on neuronal discharge', *J Neurophysiol*, 78: 3198-209.

Schofield, G. G., and S. R. Ikeda. 1988. 'Neuropeptide-Y Blocks a

Calcium Current in C-Cells of Bullfrog Sympathetic-Ganglia', *European Journal of Pharmacology*, 151: 131-34.

Seabrook, G. R., L. A. Fieber, and D. J. Adams. 1990. 'Neurotransmission in Neonatal Rat Cardiac Ganglion Insitu', *American Journal of Physiology*, 259: H997-H1005.

Seagard, J. L., F. A. Hopp, H. A. Drummond, and D. M. Van Wynsberghe. 1993. 'Selective contribution of two types of carotid sinus baroreceptors to the control of blood pressure', *Circ Res*, 72: 1011-22.

Shapiro, M. S., L. P. Wollmuth, and B. Hille. 1994. 'Modulation of Ca2+ Channels by Ptx-Sensitive G-Proteins Is Blocked by N-Ethylmaleimide in Rat Sympathetic Neurons', *Journal of Neuroscience*, 14: 7109-16.

Shen, K. Z., and A. Surprenant. 1993. 'Common Ionic Mechanisms of Excitation by Substance-P and Other Transmitters in Guinea-Pig Submucosal Neurons', *Journal of Physiology-London*, 462: 483-501.

Shibata, M., S. Einhaus, J. B. Schweitzer, S. Zuckerman, and C. W. Leffler. 1993. 'Cerebral blood flow decreased by adrenergic stimulation of cerebral vessels in anesthetized newborn pigs with traumatic brain injury', *J Neurosurg*, 79: 696-704.

Shimizu, W., Y. Tsuchioka, S. Karakawa, K. Nagata, J. Mukai, T. Yamagata, H. Matsuura, G. Kajiyama, and Y. Matsuura. 1994. 'Differential effect of pharmacological autonomic blockade on

some electrophysiological properties of the human ventricle and atrium', *Br Heart J*, 71: 34-7.

Silva, L. R. B. E., A. R. Zamuner, P. Gentil, F. M. Alves, A. G. F. Leal, V. Soares, M. S. Silva, M. F. Vieira, K. Simoes, G. R. Pedrino, and A. C. S. Rebelo. 2017. 'Cardiac Autonomic Modulation and the Kinetics of Heart Rate Responses in the On-and Off-Transient during Exercise in Women with Metabolic Syndrome', *Frontiers in Physiology*, 8.

Steele, P. A., I. L. Gibbins, J. L. Morris, and B. Mayer. 1994. 'Multiple populations of neuropeptide-containing intrinsic neurons in the guinea-pig heart', *Neuroscience*, 62: 241-50.

Stern, J. E. 2001. 'Electrophysiological and morphological properties of pre-autonomic neurones in the rat hypothalamic paraventricular nucleus', *J Physiol*, 537: 161-77.

Subhashri, S., P. Pal, G. K. Pal, D. Papa, and N. Nanda. 2020. 'Decreased baroreflex sensitivity is associated with cardiometabolic risks and prehypertension status in early-postmenopausal women', *Clin Exp Hypertens*: 1-8.

Sun, J., Y. Lu, N. Wugeti, and A. Aikemu. 2015. 'The influence of cardiac autonomic nerve plexus on the electrophysiological properties in canines with atrial fibrillation', *Int J Clin Exp Med*, 8: 4968-78.

Szpunar, M. J., E. K. Belcher, R. P. Dawes, and K. S. Madden. 2016. 'Sympathetic innervation, norepinephrine content, and norepinephrine turnover in orthotopic and spontaneous models

of breast cancer', *Brain Behav Immun*, 53: 223-33.

Tan, Z. Y., Y. J. Lu, C. A. Whiteis, A. E. Simms, J. F. R. Paton, M. W. Chapleau, and F. M. Abboud. 2010. 'Chemoreceptor Hypersensitivity, Sympathetic Excitation, and Overexpression of ASIC and TASK Channels Before the Onset of Hypertension in SHR', *Circulation Research*, 106: 536-U54.

Tapper, J., M. B. Skrifvars, R. Kivisaari, J. Siironen, and R. Raj. 2017. 'Primary decompressive craniectomy is associated with worse neurological outcome in patients with traumatic brain injury requiring acute surgery', *Surg Neurol Int*, 8: 141.

Tavernarakis, N., and M. Driscoll. 1997. 'Molecular modeling of mechanotransduction in the nematode Caenorhabditis elegans', *Annual Review of Physiology*, 59: 659-89.

Thoren, P., P. A. Munch, and A. M. Brown. 1999. 'Mechanisms for activation of aortic baroreceptor C-fibres in rabbits and rats', *Acta Physiol Scand*, 166: 167-74.

Trickey, K., L. Hornby, S. D. Shemie, and J. Teitelbaum. 2017. 'Mechanism of Death after Decompressive Craniectomy in Non-Traumatic Brain Injury', *Can J Neurol Sci*, 44: 112-15.

Tsien, R. W., D. Lipscombe, D. V. Madison, K. R. Bley, and A. P. Fox. 1988. 'Multiple types of neuronal calcium channels and their selective modulation', *Trends Neurosci*, 11: 431-8.

Tu, H. Y., J. X. Liu, D. Z. Zhang, H. Zheng, K. P. Patel, K. G. Cornish, W. Z. Wang, R. L. Muelleman, and Y. L. Li. 2014. 'Heart failure-

induced changes of voltage-gated Ca2+ channels and cell excitability in rat cardiac postganglionic neurons', *American Journal of Physiology-Cell Physiology*, 306: C132-C42.

Tu, H., L. Zhang, T. P. Tran, R. L. Muelleman, and Y. L. Li. 2010. 'Reduced expression and activation of voltage-gated sodium channels contributes to blunted baroreflex sensitivity in heart failure rats', *J Neurosci Res*, 88: 3337-49.

Vanner, S., R. J. Evans, S. G. Matsumoto, and A. Surprenant. 1993. 'Potassium Currents and Their Modulation by Muscarine and Substance-P Neuronal Cultures from Adult Guinea-Pig Celiac Ganglia', *Journal of Neurophysiology*, 69: 1632-44.

Vaseghi, M., and K. Shivkumar. 2008. 'The role of the autonomic nervous system in sudden cardiac death', *Progress in Cardiovascular Diseases*, 50: 404-19.

Vergara, C., R. Latorre, N. V. Marrion, and J. P. Adelman. 1998. 'Calcium-activated potassium channels', *Curr Opin Neurobiol*, 8: 321-9.

Vishwanath, M., S. Jafarlou, I. Shin, N. Dutt, A. M. Rahmani, M. M. Lim, and H. Cao. 2020. 'Classification of Electroencephalogram in a Mouse Model of Traumatic Brain Injury Using Machine Learning Approaches(.)', *Annu Int Conf IEEE Eng Med Biol Soc*, 2020: 3335-38.

Vlahos, R., M. E. Fabiani, and D. F. Story. 2000. 'Influence of the epithelium on acetylcholine release from parasympathetic

nerves of the rat trachea', *J Auton Pharmacol*, 20: 237-51.

von Holst, H., and X. Li. 2015. 'Higher impact energy in traumatic brain injury interferes with noncovalent and covalent bonds resulting in cytotoxic brain tissue edema as measured with computational simulation', *Acta Neurochir (Wien)*, 157: 639-48; discussion 48.

Wang, J., M. Irnaten, R. A. Neff, P. Venkatesan, C. Evans, A. D. Loewy, T. C. Mettenleiter, and D. Mendelowitz. 2001. 'Synaptic and neurotransmitter activation of cardiac vagal neurons in the nucleus ambiguus', *Ann N Y Acad Sci*, 940: 237-46.

Wehrwein, E. A., H. S. Orer, and S. M. Barman. 2016. Overview of the Anatomy, Physiology, and Pharmacology of the Autonomic Nervous System', *Compr Physiol, 13: 1239-78*.

Wharton, J. M., R. E. Coleman, and H. C. Strauss. 1992. 'The role of the autonomic nervous system in sudden cardiac death', *Trends Cardiovasc Med*, 2: 65-71.

Williams, G., D. Lai, A. Schache, and M. E. Morris. 2015. 'Classification of gait disorders following traumatic brain injury', *J Head Trauma Rehabil*, 30: E13-23.

Winchell, R. J., and D. B. Hoyt. 1997. 'Analysis of heart-rate variability: A noninvasive predictor of death and poor outcome in patients with severe head injury', *Journal of Trauma-Injury Infection and Critical Care*, 43: 927-33.

Xi-Moy, S. X., W. C. Randall, and R. D. Wurster. 1993. 'Nicotinic and muscarinic synaptic transmission in canine intracardiac

ganglion cells innervating the sinoatrial node', *J Auton Nerv Syst*, 42: 201-13.

Xi, X., W. C. Randall, and R. D. Wurster. 1991. 'Intracellular-Recording of Spontaneous Activities in Canine Intracardiac Ganglion-Cells Invitro', *Faseb Journal*, 5: A1493-A93.

Xu, Z. J., and D. J. Adams. 1992. 'Voltage-Dependent Sodium and Calcium Currents in Cultured Parasympathetic Neurons from Rat Intracardiac Ganglia', *Journal of Physiology-London*, 456: 425-41.

Yamakami, I., and T. K. McIntosh. 1989. 'Effects of traumatic brain injury on regional cerebral blood flow in rats as measured with radiolabeled microspheres', *J Cereb Blood Flow Metab*, 9: 117-24.

Yamasaki, M., T. Shimizu, M. Miyake, Y. Miyamoto, S. Katsuda, O. Ishi H, T. Nagayama, H. Waki, K. Katahira, H. Wago, T. Okouchi, S. Nagaoka, and C. Mukai. 2004. 'Effects of space flight on the histological characteristics of the aortic depressor nerve in the adult rat: electron microscopic analysis', *Biol Sci Space*, 18: 45-51.

Yuan, X. Q., D. S. Prough, T. L. Smith, and D. S. Dewitt. 1988. 'The effects of traumatic brain injury on regional cerebral blood flow in rats', *J Neurotrauma*, 5: 289-301.

Zhang, J., and S. W. Mifflin. 1998. 'Differential roles for NMDA and non-NMDA receptor subtypes in baroreceptor afferent integration in

the nucleus of the solitary tract of the rat', *J Physiol*, 511 (Pt 3): 733-45.

VIII. ABSTRACT IN KOREAN

외상성 뇌손상 쥐 모델에서
심장 자율신경기능부전의 세포 및 분자 메커니즘

오 지 웅

연세대학교 대학원 의학과

<지도교수: 황 금>

외상성 뇌 손상은 손상의 중증도와 상관없이 빈번하게 심장 자율신경기능부전 을 유발하며, 이는 환자의 유병률 및 사망률 증가와 관련이 있다. 외상성뇌손강에 의한 자율신경기능부전에 관한 세포수준의 메커니즘 규명이 중요함에도 불구하고 이와 관련된 동물 연구는 아직 이루어지지 않고 있다. 본 연구에서는 조절된 피질 충격을 가한 외상성 뇌손상 쥐 모델에서 손상 후 아급성기 때 자율신경기능부전의 발생 여부를 조사했다.

TBI의 중증도는 피질 병변 부피의 정량화를 통해 평가하였다. 심박동 변이율의 주파수 영역 의 파워 스펙트럼 분석 결과 중등도 및 중증의 외상성 뇌 손상군에서 저주파 / 고주파 비율이 증가하였다. 한편, 혈관 수축제로 유도한 압력 수용체 활성화 기간 동안 반사성 서맥을 측정한 결과 중등도 및 중증의 외상성 뇌손상군에서 압력 반사 민감도 가 감소하였다. 외상성 뇌손상군에서 관찰되는 높은 저주파 / 고주파 비율과 낮은 압력반사민감도는 교감 신경의 과도한 활성 및 부교감신경의 낮은 활성에 의한 자율신경의 불균형을 시사 하였다. 이러한 신경생리학적 현상을 세포 수준에서 확인하기 위해 그라미시딘 천공 패치 클램프 기법을 이용하여 교감 성상신경절 뉴런과 부교감 심장내신경절 뉴런에서 세포 흥분성을 기록하였다. 대조군에 비해 외상성 뇌 손상 쥐 모델에서 활동전압의 생성 빈도가 교감 성상신경절 뉴런 및 부교감 내심신경절 뉴런에서 각각에서 유의하게 증가 또는 감소되었다. 외상성 뇌 손상군에서 성상신경절 뉴런의 과흥분성과 내심신경정 뉴런의 저흥분성은 각각 활동전위 역치 및 기간의 감소 혹은 증가와 관련이 있었다. 지연정류 포타슘 전류와는 다르게 단기간 에이 형 포타슘 전류가 대조군에 비해 외상성 뇌손상 그룹의 성상신경절 뉴런에서 유의하게 감소하였다. 이러한 전기 생리학적 데이터에 일치하게 Kv4 알파 서브 유닛 (Kv4.1, Kv4.2 및 Kv4.3)을 코딩하는 전사체 발현은 대조군에 비하여 외상성 뇌 손상군의 성상신경절 뉴런에서 유의하게 감소되었다. 선택적 엠 형 포타슘 채널 길항제인 XE-991을 가햇을 때 성상신경절 및 내심신경절 뉴

런에서 활동전위 생성 빈도가 증가하였다. 외상성 뇌 손상은 기능적 엠형 포타슘 전류 및 KCNQ2 전사체의 하향 조절 및 상향 조절하였는데 이들은 각각 성상신경절 뉴런의 과흥분성 및 내심신경절 뉴런의 저흥분성에 각각 기여할 것이다. 이밖에도 외상성 뇌 손상은 혈압 반사궁의 감각신경 축에도 영향을 주어 에형 및 씨 형 압력반사뉴런의 흥분성을 극적으로 감소시켰다.

결론적으로 뇌손상 쥐 모델에서 자율신경기능부전은 뇌손상후 아급성 기간에 나타났다. 이러한 외상성 뇌손상에 의한 자율신경기능 부전의 핵심 기전은 KA 및 KM 채널 전류의 조절에 의한 말초 심장 원심성 뉴런의 기능적 가소성과 심장 구심성 뉴런의 기능적 가소성 일 것으로 사료된다.

핵심 되는 말: 교감 신경, 부교감 신경, 성상신경절, 심박동 변이율, 심장내신경절, 심혈관 자율 신경 기능 장애, 압력 반사 민감성, 외상성 뇌손상, 자율 신경 기능 장애, 칼륨 채널